Measurement of the F_2^n/F_2^p, d/u **RA**tios and A=3 EMC Effect in Deep Inelastic Electron Scattering Off the **T**ritium and **H**elium Mirr**O**r **N**uclei.

Jefferson Lab PAC37 Proposal, December 2010

The JLab **MARATHON** Collaboration

J. Arrington, D. F. Geesaman, K. Hafidi, R. J. Holt, D. Potterveld, P. Reimer, J. Rubin, J. Singh, X. Zhan
Argonne National Laboratory, Argonne, Illinois, USA

K. A. Aniol, D. J. Margaziotis, M. B. Epstein
California State University, Los Angeles, California, USA

G. Fanourakis
Demokritos National Center for Scientific Research, Athens, Greece

J. Annand, D. Ireland, R. Kaiser, G. Rosner
University of Glasgow, Scotland, UK

E. Cisbani, F. Cussano, S. Frullani, F. Garibaldi, M. Iodice, L. Lagamba, R. De Leo, E. Pace, G. Salmè, G. M. Urciuoli
Istituto Nazionale di Fisica Nucleare, Rome and Bari, Italy

J.-P. Chen, E. Chudakov, J. Gomez, J.-O. Hansen, D. W. Higinbotham, C. W. de Jager, J. LeRose, D. Meekins, W. Melnitchouk, R. Michaels, S. K. Nanda, B. Sawatsky, P. Solvignon, A. Saha, B. Wojtsekhowski
Jefferson Lab, Newport News, Virginia, USA

B. D. Anderson, A. T. Katramatou, D. M. Manley, S. Margetis, G. G. Petratos, W.-M. Zhang
Kent State University, Kent, Ohio, USA

W. Korsch
University of Kentucky, Lexington, Kentucky, USA

X. Jiang, A. Puckett
Los Alamos National Laboratory, Los Alamos, New Mexico, USA

E. Beise
University of Maryland, College Park, Maryland, USA

J. R. Calarco, K. Slifer
University of New Hampshire, Durham, New Hampshire, USA

C. Ciofi degli Atti, S. Scopetta
University of Perugia, Perugia, Italy

R. Gilman, R. D. Ransome
Rutgers, The State University of New Jersey, New Brunswick, New Jersey, USA

M. N. Olson
St. Norbert College, De Pere, Wisconsin, USA

N. Sparveris
Temple University, Philadelphia, Pennsylvania, USA

D. Day, S. Liuti, O. Rondon
University of Virginia, Charlottesville, Virginia, USA

Spokesperson: G. G. Petratos (gpetrato@kent.edu)
Co-spokespersons: J. Gomez, R. J. Holt and R. D. Ransome

ABSTRACT

This is an updated proposal for the twice conditionally approved E12-010-103 JLab Experiment. It was originally proposed, as PR12-06-118 in 2006, and reviewed by PAC30, which considered "the physics goals of this experiment as highlights of the 12 GeV physics program." The condition for (full) approval imposed by PAC30 was a "Management review of the safety aspects of the Tritium target." A review of a conceptual target design was conducted in June 2010, which found "no show stoppers" for further development of a low activity tritium target at Jefferson Lab. The outcome of the review allowed the resubmission of the proposal to PAC36, which, per preliminary PAC-closeout communication, reaffirmed the scientific importance of the experiment but imposed a full detector design for the Super BigBite Spectrometer as a condition for (full) approval.

We propose to perform deep inelastic electron scattering off the ^{3}H and ^{3}He mirror nuclei with the 11 GeV upgraded beam of Jefferson Lab. The experiment will measure the EMC effect for ^{3}H and ^{3}He and determine the ratio of the neutron to proton inelastic structure functions, F_2^n/F_2^p, and the ratio of the down to up quark distributions in the nucleon, d/u, at medium and large Bjorken x. It will use a room-temperature, moderate-pressure ^{3}H, ^{3}He and deuterium gas target system, and the Hall A BigBite (*instead of the Super BigBite*) and the Left High Resolution Spectrometers. The tested and successfully operated BigBite Spectrometer will be used in its standard electron detection configuration with modifications to its Cherenkov counter. The required beam time is 42 days at a beam current of 25 μA. The F_2^n/F_2^p ratio will be extracted from the inelastic cross section ratio of the two nuclei by exploiting their mirror symmetry with a minimal theoretical correction. The F_2^n/F_2^p ratio is expected to be almost free of nuclear effects, which introduce a significant uncertainty in its extraction from deep inelastic scattering off the proton and deuteron. The results are expected to test perturbative and non-perturbative mechanisms of spin-flavor symmetry breaking in the nucleon, and constrain the structure function parametrizations needed for the interpretation of high energy hadron collider and neutrino oscillations data. The precision of the expected data for the ratio of the EMC effects for ^{3}H and ^{3}He will offer a unique opportunity to test theoretical calculations of the EMC effect and will provide critical experimental input for the establishment of a unique canonical model for the explanation of its dynamical origin.

1 Introduction

Measurements of the proton and deuteron structure functions have been of fundamental importance in establishing the internal quark structure of the nucleon [1, 2, 3]. The first evidence for the presence of point-like constituents (partons) in the nucleon came from the observation that the ratio of inelastic to Mott electron-proton cross sections, measured in the pioneering SLAC experiments, exhibited only small variation with momentum transfer [4]. The subsequent detailed analysis of the SLAC data [5] revealed the predicted "scaling pattern" [6] in the nucleon structure functions, consistent with scattering from partons carrying the quantum numbers of the Gell-Mann/Zweig quarks. Further experimental studies of muon-nucleon and neutrino-nucleon inelastic scattering experiments at CERN and Fermilab established beyond any doubt the quark-parton model (QPM) of the nucleon [7], and provided substantial supporting evidence for the emerging theory of quantum chromodynamics (QCD) [8]. The importance of the SLAC experiments for the development of the quark model in particle physics was recognized with the 1990 Nobel in Physics award to J. Friedman, H. Kendall and R. Taylor.

The cross section for inelastic electron-nucleon scattering is given in terms of the structure functions $F_1(\nu, Q^2)$ and $F_2(\nu, Q^2)$ of the nucleon by:

$$\sigma \equiv \frac{d^2\sigma}{d\Omega dE'}(E, E', \theta) = \frac{4\alpha^2 (E')^2}{Q^4} \cos^2(\frac{\theta}{2}) \left[\frac{F_2(\nu, Q^2)}{\nu} + \frac{2F_1(\nu, Q^2)}{M} \tan^2(\frac{\theta}{2}) \right] , \qquad (1)$$

where α is the fine-structure constant, E is the incident electron energy, E' and θ are the scattered electron energy and angle, $\nu = E - E'$ is the energy transfer, $Q^2 = 4EE' \sin^2(\theta/2)$ is minus the four-momentum transfer squared, and M is the nucleon mass.

The basic idea of the quark-parton model [6, 9] is to represent inelastic electron-nucleon scattering as quasi-free scattering from the partons/quarks in the nucleon, when viewed in a frame where the nucleon has infinite momentum (the center-of-mass frame is a very good approximation to such a frame). The fractional momentum of the nucleon carried by the struck quark is given by the Bjorken scaling variable, $x = Q^2/2M\nu$. In the limit where $\nu \to \infty$, $Q^2 \to \infty$ with x fixed, the nucleon structure functions become:

$$F_1 = \frac{1}{2} \sum_i e_i^2 q_i(x) , \qquad F_2 = x \sum_i e_i^2 q_i(x) . \qquad (2)$$

Here, e_i is the fractional charge of quark type i, $q_i(x)dx$ is the probability that a quark of type i carries momentum in the range between x and $x + dx$, and the sum runs over all quark types.

Since the charges of the u, d and s quarks are $2/3$, $-1/3$ and $-1/3$, respectively, the $F_2(x)$ structure function for the proton is given by:

$$F_2^p(x) = x\left[\left(\frac{2}{3}\right)^2(u+\bar{u}) + \left(-\frac{1}{3}\right)^2\left(d+\bar{d}\right) + \left(-\frac{1}{3}\right)^2(s+\bar{s})\right]. \tag{3}$$

The parton distribution functions in the neutron are related to those in the proton by isospin symmetry. Since the up/down quarks and proton/neutron both form isospin doublets, one has: $u^p(x) = d^n(x) \equiv u(x)$, $d^p(x) = u^n(x) \equiv d(x)$, $s^p(x) = s^n(x) \equiv s(x)$ (with analogous relations for the antiquarks), and:

$$F_2^n(x) = x\left[\left(-\frac{1}{3}\right)^2(u+\bar{u}) + \left(\frac{2}{3}\right)^2\left(d+\bar{d}\right) + \left(-\frac{1}{3}\right)^2(s+\bar{s})\right]. \tag{4}$$

Equations 3 and 4 result in the structure function ratio:

$$\frac{F_2^n}{F_2^p} = \frac{[(u+\bar{u})+(s+\bar{s})]+4(d+\bar{d})}{4(u+\bar{u})+[(d+\bar{d})+(s+\bar{s})]}\ . \tag{5}$$

Since all the quark distribution functions must be positive for all x, the above expression is bounded for all x by:

$$\frac{1}{4} \leq \frac{F_2^n}{F_2^p} \leq 4\ , \tag{6}$$

which is known as the Nachtmann inequality [10]. If one neglects the strange quarks and antiquarks, Equation 5 yields the well known simple relationship:

$$\frac{F_2^n}{F_2^p} = \frac{[(u+\bar{u})]+4(d+\bar{d})}{4(u+\bar{u})+[(d+\bar{d})]} = \frac{1+4(D/U)}{4+(D/U)}\ , \tag{7}$$

where $U = u + \bar{u}$ and $D = d + \bar{d}$. For the remainder of this proposal the notation D/U will be replaced, as it is customary, simply by d/u, with d and u denoting quark plus antiquark distributions. Figure 1 shows all the SLAC data from the pioneering SLAC/MIT Collaboration experiments on the F_2^n/F_2^p ratio versus x [11]. The ratio has been extracted from deep inelastic scattering (DIS) (large Q^2 and ν) measurements off the proton and deuteron, using a smearing model to account for the Fermi-motion of the nucleons in the deuteron [12]. The ratio data are within the bounds of the Nachtmann inequality. For large x, the ratio is about $1/4$ which can only be reached if $d = s = 0$. This suggests a picture in which the high momentum partons in the proton (neutron) are mainly up (down) quarks. For small x, the ratio is close to 1, suggesting little influence of valence quarks and dominance of the quark-antiquark "sea".

Early SLAC experimental data in a limited x kinematical range ($0.1 \leq x \leq 0.3$) [13] reinforced an original naive view that the quark distributions functions $q_i(x)$ should not

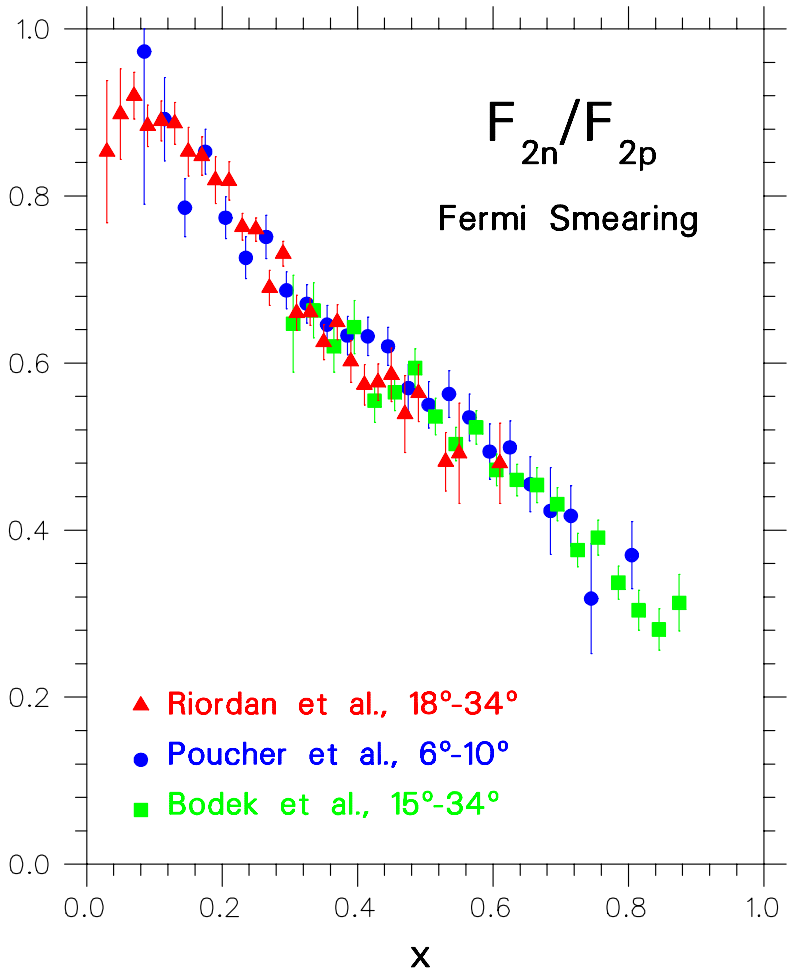

Figure 1: SLAC data on the nucleon F_2^n/F_2^p ratio extracted from proton and deuteron DIS measurements [11] with a Fermi-smearing model [12].

change in the nuclear medium, at least for small and medium values of x. Measurements by the European Muon Collaboration (EMC) [14] over a large-x range at CERN invalidated this view by observing a large x dependence for the ratio of the iron F_2^{Fe} per nucleon over the deuteron F_2^d. This effect, the EMC effect, was confirmed in a subsequent analysis of old SLAC data [15], and an extensive study, using different nuclear targets, provided the exact x behavior of the effect versus the mass number A of nuclei [16]. The SLAC experimental data are shown in Figure 2 and indeed indicate a significant x and A dependence for the inelastic cross section ratio $(\sigma^A/\sigma^d)_{is}$ for several nuclei from ^{4}He to Au. The σ^A and deuteron σ^d cross sections are per nucleon and the ratio has been adjusted for an isoscalar nucleus of mass number A. This cross section ratio is equal to the equivalent isoscalar structure function ratio $(F_2^A/F_2^d)_{is}$.

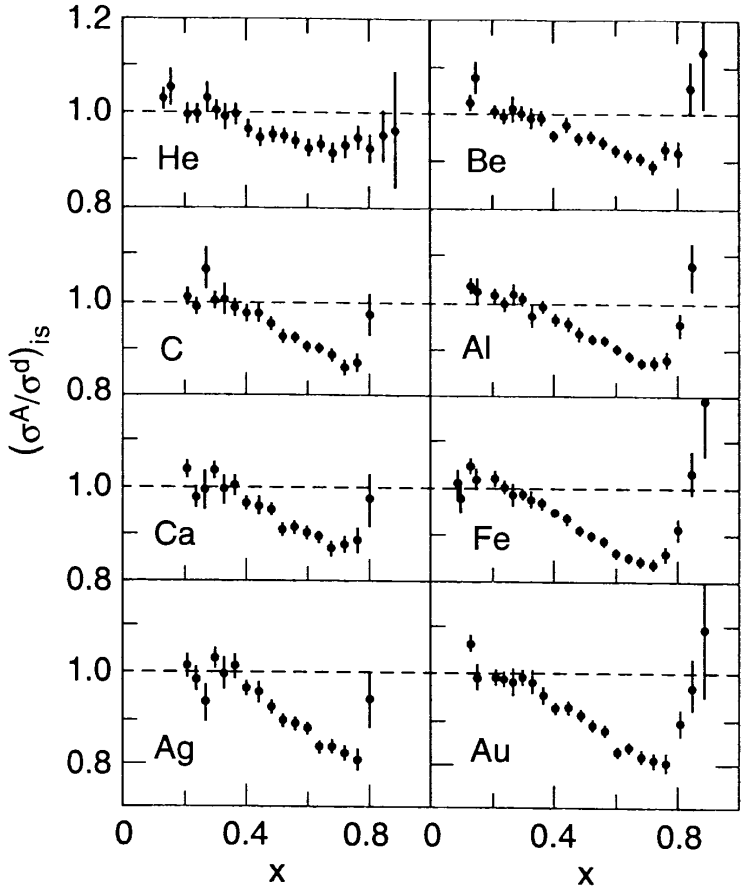

Figure 2: SLAC data on the inelastic cross section ratio of several nuclei (σ^A) to deuterium (σ^d) versus the Bjorken x [16]. The cross sections are per nucleon and the ratio has been adjusted for an isoscalar nucleus of mass number A.

2 Theory Overview

The F_2^n/F_2^p ratio can be calculated in a number of models of the nucleon. In a world of exact SU(6) symmetry, the wave function of a proton, polarized in the $+z$ direction for instance, would be simply [7]:

$$\begin{aligned} p\uparrow \;=\; & \frac{1}{\sqrt{2}}u\uparrow(ud)_{S=0} \;+\; \frac{1}{\sqrt{18}}u\uparrow(ud)_{S=1} \;-\; \frac{1}{3}u\downarrow(ud)_{S=1} \\ & -\frac{1}{3}d\uparrow(uu)_{S=1} \;-\; \frac{\sqrt{2}}{3}d\downarrow(uu)_{S=1}\;, \end{aligned} \tag{8}$$

where the subscript S denotes the total spin of the "diquark" partner of the quark. In this limit, the u and d quarks in the proton would be identical, and the nucleon and Δ

isobar would, for example, be degenerate in mass. In deep-inelastic scattering, exact SU(6) symmetry would be manifested in equivalent shapes for the valence quark distributions of the proton, which would be related simply by $u(x) = 2d(x)$ for all x. For the neutron to proton F_2 structure function ratio this would imply [17]:

$$\frac{F_2^n}{F_2^p} = \frac{2}{3}, \qquad \frac{d}{u} = \frac{1}{2} \qquad \text{[SU(6) symmetry]}. \tag{9}$$

In nature, spin-flavor SU(6) symmetry is, of course, broken. The nucleon and Δ masses are split by some 300 MeV. In deep inelastic scattering off the nucleon, this symmetry breaking is reflected in the experimental observation that the d quark distribution is softer than the u quark distribution, with the F_2^n/F_2^p ratio deviating from the SU(6) expectation. The correlation between the mass splitting in the **56** baryons and the large-x behavior of F_2^n/F_2^p was observed some time ago by Close [18] and Carlitz [19]. Based on phenomenological [18] and Regge [19] arguments, the breaking of the symmetry in Equation 8 was argued to arise from a suppression of the "diquark" configurations having $S = 1$ relative to the $S = 0$ configuration as $x \to 1$. Such a suppression is in fact quite natural if one observes that whatever mechanism leads to the observed $N - \Delta$ splitting (*e.g.* color-magnetic force, instanton-induced interaction, pion exchange), it necessarily acts to produce a mass splitting between the two possible spin states of the two quarks which act as spectators to the hard collision, $(qq)_S$, with the $S = 1$ state heavier than the $S = 0$ state by some 200 MeV [20]. From Equation 8, a dominant scalar valence diquark component of the proton suggests that in the $x \to 1$ limit, F_2^p is essentially given by a single quark distribution (i.e. the u), in which case:

$$\frac{F_2^n}{F_2^p} \to \frac{1}{4}, \qquad \frac{d}{u} \to 0 \qquad [S = 0 \text{ dominance}]. \tag{10}$$

This expectation has, in fact, been built into most phenomenological fits to the parton distribution data [21, 22, 23, 24].

The phenomenological suppression of the d quark distribution can be understood within the hyperfine-perturbed quark model of Isgur *et al.* [25, 26]. The color hyperfine interaction is generated by one-gluon exchange between quarks in the core. At lowest order, the Hamiltonian for the color-magnetic hyperfine interaction between two quarks is proportional to $\vec{S}_i \cdot \vec{S}_j$, where $\vec{S}_i$ is the spin vector of quark i. Because this force is repulsive if the spins of the quarks are parallel and attractive if they are antiparallel, from the SU(6) wave function in Equation 8 it naturally leads to an increase in the mass of the Δ and a lowering of the mass of the nucleon, and a softening of the d quark distribution relative to the u [26].

An alternative suggestion, based on a perturbative QCD argument, was originally formulated by Farrar and Jackson [27]. There it was shown that the exchange of longitudinal gluons, which are the only type permitted when the spins of the two quarks in $(qq)_S$ are aligned, would introduce a factor $(1-x)^{1/2}$ into the Compton amplitude — in comparison with the exchange of a transverse gluon between quarks with spins anti-aligned. In this approach, the relevant component of the proton valence wave function at large x is that associated with states in which the total "diquark" spin projection, S_z, is zero as $x \to 1$. Consequently, scattering from a quark polarized in the opposite direction to the proton polarization is suppressed by a factor $(1-x)$ relative to the helicity-aligned configuration.

A similar result is also obtained in the treatment of Brodsky *et al.* [28] (based on quark-counting rules), where the large-x behavior of the parton distribution for a quark polarized parallel ($\Delta S_z = 1$) or antiparallel ($\Delta S_z = 0$) to the proton helicity is given by: $q^{\uparrow\downarrow}(x) = (1-x)^{2n-1+\Delta S_z}$, where n is the minimum number of non-interacting quarks (equal to 2 for the valence quark distributions). Using Equation 8, in the $x \to 1$ limit one therefore predicts:

$$\frac{F_2^n}{F_2^p} \;\to\; \frac{3}{7}, \qquad \frac{d}{u} \to \frac{1}{5} \qquad [S_z = 0 \text{ dominance}]. \tag{11}$$

It should be noted that in the latter two treatments, the d/u ratio does not vanish as $x \to 1$ and the F_2^n/F_2^p ratio tends to 3/7 instead of 1/4.

Moving to the EMC effect, despite the intense theoretical work over the 20 years since its discovery, there is no unique theory or universally accepted model that describes its origin. There are many classes of models offering possible explanations of the effect. One class tries to explain the effect by revisiting the bound-nucleon problem and offering refined treatments for the nuclear binding and nucleon off-shellness. A second class attributes the existence of the effect to a possible increasing enhancement of the pion field, associated with the nucleon-nucleon interaction, with the nuclear mass number A. A third class departs from the conventional meson-nucleon framework of the nucleus and assumes that a dense nucleus with tightly packed nucleons has to be viewed and treated as a collection of multi-quark clusters. A distinct model in this class is one offering a quark-diquark structure of the nucleon, with the diquark modified in the nuclear medium. A fourth class is based on the idea of dynamical rescaling arising from the observation that iron F_2 structure function data resemble deuterium F_2 structure function data of higher Q^2 values. The underlying physical idea in this rescaling model is the change in the quark confinement scale of a nucleon embedded in a nucleus.

The above four classes are sometimes complemented by additional mechanisms that can offer explanations for the EMC effect pattern in specific x regions, like the well known shadowing mechanism, which reproduces the low-x pattern of the effect, and the increased Fermi momentum of the nucleons in heavier nuclei, which accounts for the large-x behavior of the EMC ratio data. The large number of approaches and models trying to explain the effect as well as comprehensive detailed accounts and comparisons of theoretical calculations with data are given in the excellent reviews of Refs. [29, 30].

It is widely accepted that the first step in the understanding of the origin of the EMC effect is a realistic calculation of the structure function F_2 of the light, simplest nuclei in nature and in particular of the $A = 3$ mirror nuclei: ^{3}He and ^{3}H. Of paramount importance would be a comparison of theory and experimental data for the ratio of the structure functions of the two nuclei, where both systematic and theoretical inherent uncertainties cancel out, making this ratio a benchmark for the understanding of the EMC effect [31].

3 Motivation for a New Experiment

Although the problem of extracting neutron structure functions from deuterium data is rather old [32], the discussion has been recently revived [33, 34, 35] with the realization [36] that F_2^n, extracted from F_2^p and F_2^d by taking into account Fermi-motion *and* binding effects in deuterium, could be significantly different [34, 36] from that extracted in earlier analyses [12] in which only Fermi-motion corrections were applied.

Melnitchouk and Thomas [34] have incorporated binding and off-shell effects within a covariant framework in terms of relativistic deuteron wave functions (as calculated by Gross and collaborators [37], for instance). Neglecting the relativistic deuteron P-states and off-shell deformation of the bound nucleon structure function (which were found to contribute at the $\sim 1\%$ level [38]), the deuteron F_2^d structure function can be written as a convolution of the free proton and neutron F_2 structure functions and a nucleon momentum distribution in the deuteron, $f_{N/d}$:

$$F_2^d(x, Q^2) = \int dy \; f_{N/d}(y) \; [F_2^p(x/y, Q^2) + F_2^n(x/y, Q^2)], \tag{12}$$

where y is the fraction of the 'plus'-component of the nuclear momentum carried by the interacting nucleon, and $f_{N/d}(y)$ takes into account both Fermi-motion and binding effects. Their reanalysis of the SLAC data based upon this improved theoretical treatment led to

larger F_2^n/F_2^p values as compared with the Fermi-motion only extracted values. As can be seen in Figure 3, the difference at $x = 0.85$ can be up to $\sim 50\%$.

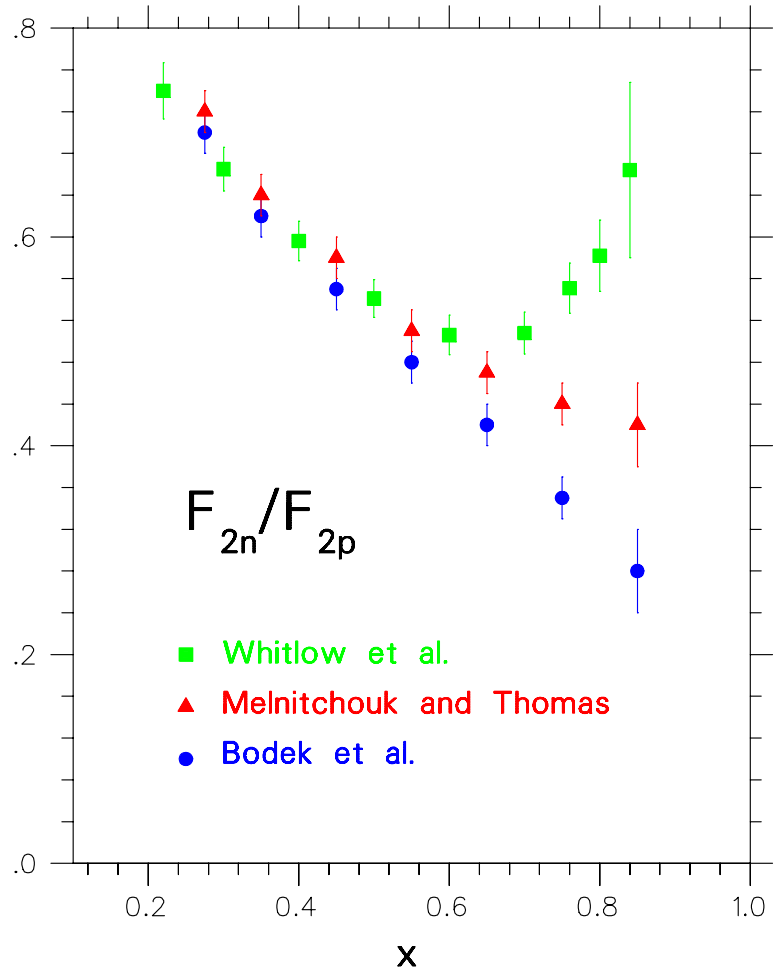

Figure 3: The F_2^n/F_2^p ratio extracted from proton and deuteron DIS measurements [11] with a) a Fermi-smearing model (Bodek *et al.* [12]), b) a covariant model that includes binding and off-shell effects (Melnitchouk and Thomas [34]), and c) the "nuclear density model" [39] that also incorporates binding and off-shell effects (Whitlow *et al.* [36]).

Whitlow *et al.* [36] incorporated binding effects using the "nuclear density model" of Frankfurt and Strikman [39]. In this model, the EMC effect for the deuteron scales with nuclear density as for heavy nuclei:

$$\frac{F_2^d}{F_2^p + F_2^n} = 1 + \frac{\rho_d}{\rho_A - \rho_d}\left[\frac{F_2^A}{F_2^d} - 1\right] \ , \tag{13}$$

where ρ_d is the charge density of the deuterium nucleus, and ρ_A and F_2^A refer to a heavy nucleus with atomic mass number A. This model predicts for the ratio F_2^n/F_2^p values that

are significantly higher ($> 100\%$) than the Fermi-motion only extracted ones at high x, as can be seen in Figure 3.

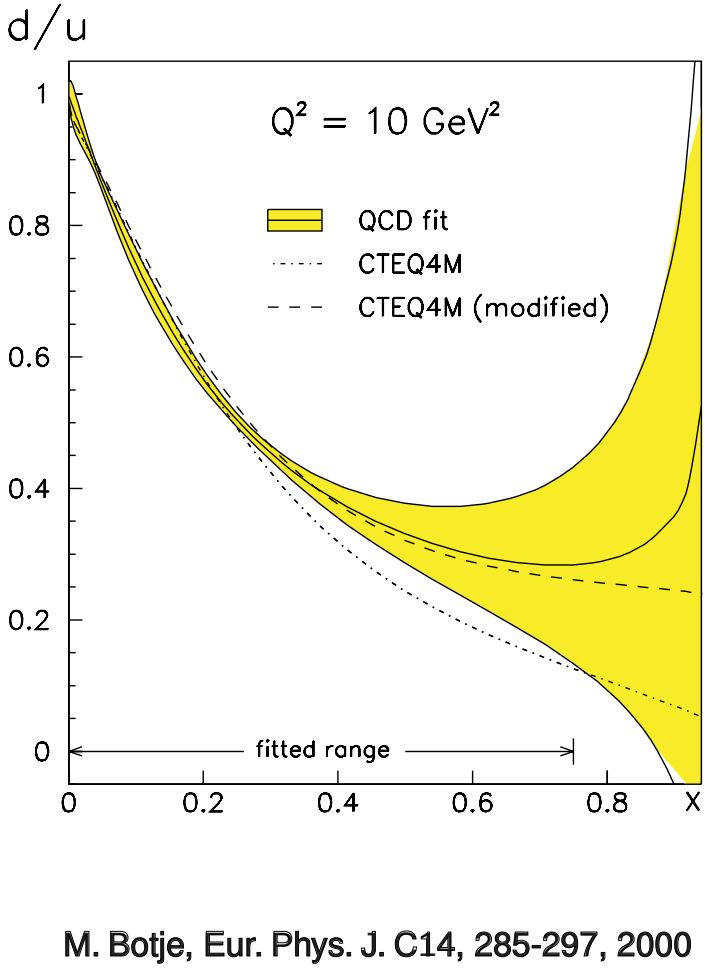

Figure 4: A typical uncertainty in the determination of the quark d/u distribution ratio by the QCD fit of Botje [40] on DIS cross section data. The solid curve is a QCD fit, and the shaded area shows the uncertainty in the fit. The dot-dashed curve represents the standard CTEQ4 fit [43], while the dashed curve corresponds to the CTEQ4 fit with a modified d quark distribution with $d/u \to \approx 0.2$ as $x \to 1$.

It is evident from the above two models that neglecting nuclear binding effects in the deuteron can introduce, at large x, a significant uncertainty in the extraction of the F_2^n/F_2^p and d/u ratios. A typical example for the magnitude of the uncertainty for the d/u ratio, as estimated by one calculation from a QCD fit of proton and deuteron structure function data, is given in Figure 4 [40] (see also Ref. [41]). The more recent CTEQ6X analysis [42] gave a similarly large spread for the d quark distribuion above $x \sim 0.5$, depending on

which assumptions about the nuclear corrections in deuterium were used. In the absence of experimental data or a unique theory for the magnitude of binding effects and the existence of the EMC effect in the deuteron, the question of the large-x behavior of F_2^n/F_2^p and d/u can only be settled by a measurement which does not rely on the use of the deuteron as an effective neutron target.

The above situation can be remedied by using a method proposed by Afnan *et al.* [44, 45], which maximally exploits the mirror symmetry of $A = 3$ nuclei and extracts the F_2^n/F_2^p ratio from DIS measurements off ^{3}H and ^{3}He. Regardless of the absolute values of the nuclear EMC effects in ^{3}He or ^{3}H, the differences between these will be small – on the scale of charge symmetry breaking in the nucleus – which allows for a determination of the F_2^n/F_2^p and d/u ratios at large-x values essentially free of nuclear contamination. At the same time, precise DIS measurements off ^{3}H and ^{3}He will provide the necessary structure function F_2 data for detailed studies of the EMC effect, which could lead to a canonical theory for the explanation of its dynamical origin. In summary, this method will, as has been stated in Ref. [31], i) unambiguously determine the valence u and d quark distributions of the free nucleon, ii) complete our knowledge of the EMC effect over the full range of nuclear mass number by determining the effect in the three-body systems and in the deuteron, and iii) provide valuable input in sorting out the change of the nucleon structure in the nuclear medium, which is fundamental to our understanding of QCD itself.

4 Exploring Deep Inelastic Scattering off ^{3}H and ^{3}He

In the absence of a Coulomb interaction and in an isospin-symmetric world, the properties of a proton (neutron) bound in the ^{3}He nucleus would be identical to that of a neutron (proton) bound in the ^{3}H nucleus. If, in addition, the proton and neutron distributions in ^{3}He (and in ^{3}H) were identical, the neutron structure function could be extracted with no nuclear corrections, regardless of the size of the EMC effect in ^{3}He or ^{3}H separately.

In practice, ^{3}He and ^{3}H are of course not perfect mirror nuclei – their binding energies for instance differ by some 10% – and the proton and neutron distributions are not quite identical. However, the $A = 3$ system has been studied for many years, and modern realistic $A = 3$ wave functions are known to rather good accuracy. In a self-consistent framework one can use the same nucleon-nucleon (NN) interaction which describes the two-nucleon system to provide the basic input interaction into the three-nucleon calculation. Therefore,

the wave functions can be tested against a large array of observables which put rather strong constraints on the models.

Defining the EMC-type ratios for the F_2 structure functions of ^{3}He and ^{3}H (weighted by corresponding isospin factors) by:

$$R(^3\mathrm{He}) = \frac{F_2^{^3\mathrm{He}}}{2F_2^p + F_2^n} \ , \qquad R(^3\mathrm{H}) = \frac{F_2^{^3\mathrm{H}}}{F_2^p + 2F_2^n} \ , \tag{14}$$

one can write the "super-ratio", $\mathcal{R}$, of these as:

$$\mathcal{R} \ = \ \frac{R(^3\mathrm{He})}{R(^3\mathrm{H})} \ . \tag{15}$$

Inverting this expression directly yields the ratio of the free neutron to proton structure functions:

$$\frac{F_2^n}{F_2^p} \ = \ \frac{2\mathcal{R} - F_2^{^3\mathrm{He}}/F_2^{^3\mathrm{H}}}{2F_2^{^3\mathrm{He}}/F_2^{^3\mathrm{H}} - \mathcal{R}} \ . \tag{16}$$

We stress that F_2^n/F_2^p extracted via Equation 16 does not depend on the size of the EMC effect in ^{3}He or ^{3}H, but rather on the *ratio* of the EMC effects in ^{3}He and ^{3}H. If the neutron and proton distributions in the $A = 3$ nuclei are not dramatically different, one might expect $\mathcal{R} \approx 1$. To test whether this is indeed the case requires an explicit calculation of the EMC effect in the $A = 3$ system.

The conventional approach employed in calculating nuclear structure functions in the valence quark region, $x > 0.3$, is the impulse approximation, in which the virtual photon, γ^*, mediating the electron-nucleus interaction, scatters incoherently from individual nucleons in the nucleus [29]. The nuclear cross section is determined by factorizing the γ^*–nucleus interaction into γ^*–nucleon and nucleon–nucleus amplitudes. The structure function of a nucleus, F_2^A, can then be calculated by folding the nucleon structure function, F_2^N, with the nucleon momentum distribution in the nucleus, $f_{N/A}$, as in Equation 12:

$$F_2^A(x) \ = \ \int dy \ f_{N/A}(y) \ F_2^N(x/y) \ \equiv \ f_{N/A}(x) \otimes F_2^N(x) \ , \tag{17}$$

where the Q^2 dependence in the structure functions is implicit. The convolution expression in Equation 17 is correct in the limit of large Q^2; at finite Q^2 the nucleon momentum distribution function $f_{N/A}$ aquires additional dependence on the variable $\gamma = \sqrt{1 + 4M^2x^2/Q^2}$ [46, 47]. While making the convolution expressions somewhat more complicated at finite Q^2, these corrections can nevertheless be straightforwardly computed. Corrections to the impulse approximation appear in the guise of final state interactions, multiple rescattering (nuclear

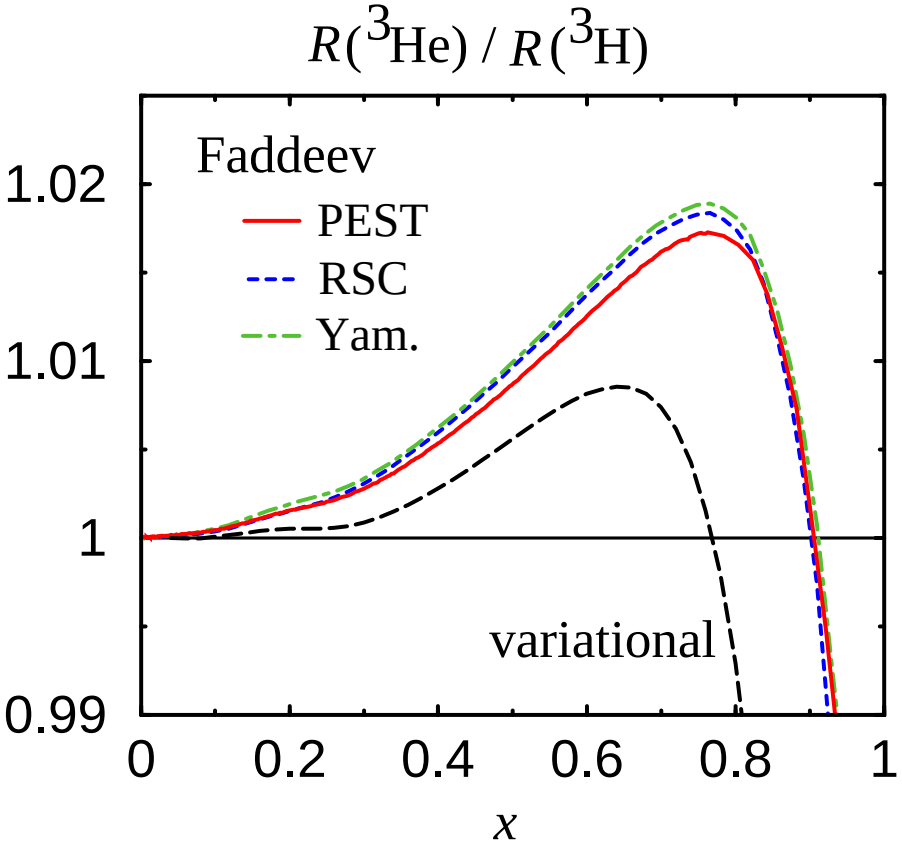

Figure 5: The "super-ratio" $\mathcal{R}$ of nuclear EMC ratios for ^{3}He and ^{3}H nuclei, with the nucleon momentum distribution calculated from the Faddeev (PEST, RSC, Yamaguchi) and variational (RSC) wave functions [45].

shadowing), NN correlations and 6-quark clusters, however, these are generally confined to either the small-x [48], or very large-x ($x > 0.9$) [49] regions.

In the high-Q^2 limit the distribution $f(y)$ of nucleons in the nucleus is related to the nucleon spectral function $S(p)$ by [29]:

$$f(y) = \int d^3\vec{p} \left(1 + \frac{p_z}{p_0}\right) \delta\left(y - \frac{p_0 + p_z}{M}\right) S(p) \ , \tag{18}$$

where p is the momentum of the bound nucleon (for a generalization to finite Q^2 see for example Ref. [46]). For an $A = 3$ nucleus the spectral function is evaluated from the three-body nuclear wave function, calculated by either solving the homogeneous Faddeev equation with a given two-body interaction [44, 50] or by using a variational technique [51]. The model dependence of the distribution function can be examined by using several different potentials. In Refs. [44, 45] a number of potentials were used, including the "EST" (Ernst-Shakin-

Thaler) separable approximation to the Paris potential [52] [referred to as "Paris (EST)"], the unitary pole approximation [53] to the Reid Soft Core (RSC) potential, and the Yamaguchi potential [54] with 7% mixing between $^3S_1$ and $^3D_1$ waves. The Argonne AV18 potential [56] was also used for the calculations in Refs. [55, 57].

In terms of the proton and neutron momentum distributions, the F_2 structure function for ^{3}He is given by:

$$F_2^{^3\mathrm{He}} \;=\; 2\, f_{p/^3\mathrm{He}} \,\otimes\, F_2^p \;+\; f_{n/^3\mathrm{He}} \,\otimes\, F_2^n \;. \tag{19}$$

Similarly for ^{3}H, the structure function is evaluated from the proton and neutron momentum distributions in ^{3}H:

$$F_2^{^3\mathrm{H}} \;=\; f_{p/^3\mathrm{H}} \otimes\, F_2^p \;+\; 2\, f_{n/^3\mathrm{H}} \otimes\, F_2^n \;. \tag{20}$$

Because isospin symmetry breaking effects in nuclei are quite small, one can to a good approximation relate the proton and neutron distributions in ^{3}He to those in ^{3}H:

$$f_{n/^3\mathrm{H}} \approx f_{p/^3\mathrm{He}} \;, \qquad f_{p/^3\mathrm{H}} \approx f_{n/^3\mathrm{He}} \;, \tag{21}$$

although in practice both the isospin symmetric and isospin symmetry breaking cases have been considered explicitly. Note that even in the isospin symmetric case the proton and neutron distributions in ^{3}He will be different because while the neutron in ^{3}He is accompanied by a spectator pp, the spectator system of the proton is either an uncorrelated pn pair or a recoiling deuteron.

The ratio $\mathcal{R}$ of EMC ratios for ^{3}He and ^{3}H, as calculated by Afnan *et al.* [44, 45] is shown in Figure 5 for the various nuclear model wave functions [Paris (EST), RSC and Yamaguchi], using the CTEQ parametrization [24] of parton distributions at $Q^2 = 10$ (GeV/c)^2 for F_2^N. The EMC effects are seen to largely cancel over a large range of x, out to $x \sim 0.9$, with the deviation from unity of less than 2%. Furthermore, the dependence on the nuclear wave function is very weak. The pattern of behavior of the ratio $\mathcal{R}$ has been confirmed in independent calculations by Pace *et al.* [55], using a variational approach to calculate the three-body spectral function, and by Sargsian *et al.* [57] using the Green function Monte Carlo wave functions from Ref. [56].

As seen in Figure 6, the deviation of $\mathcal{R}$ from unity is also well within the 2% range for both of the above cases. Note that the solid curve (from the work of Ciofi degli Atti and Liuti [58]) is computed using the RSC NN potential with the CTEQ parametrization of the

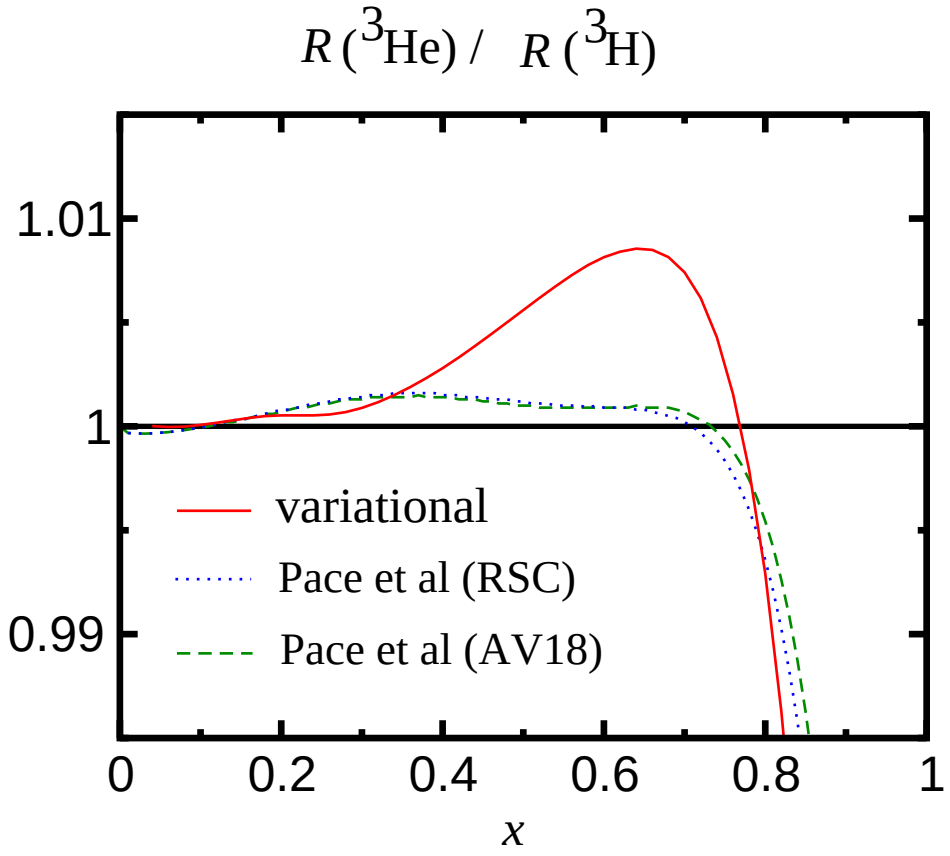

Figure 6: Ratio of nuclear EMC ratios for ^{3}He and ^{3}H for the variational calculation [45] (solid) and from Ref. [55] for the RSC (dotted) and AV18 (dashed) NN potentials (see text).

nucleon structure function, while the dashed and dotted curves (from Pace *et al.* [55]) use the RSC and Argonne AV18 nucleon-nucleon potentials with the structure function fits from Ref. [59].

The dependence of $\mathcal{R}$ on the input nucleon structure function parametrization is illustrated in Figure 7, where several representative curves at $Q^2 = 10$ (GeV/c)^2 are given: apart from the standard CTEQ fit (solid), the results for the GRV [60] (dot-dashed), Donnachie-Landshoff (DL) [61] (dashed), and BBS [28] (dotted) parametrizations are also shown (the latter at $Q^2 = 4$ (GeV/c)^2). For $x < 0.6$ there is little dependence ($< 0.5\%$) in the ratio on the structure function input. For $0.6 < x < 0.85$ the dependence is greater, but still with $< \pm 1\%$ deviation away from the central value $\mathcal{R} = 1.01$. The spread in this region is due mainly to the poor knowledge of the neutron structure function at large x. Beyond $x \approx 0.85$ there are few data in the deep-inelastic region on either the neutron or the proton structure functions, so here both the d and u quark distributions are poorly determined.

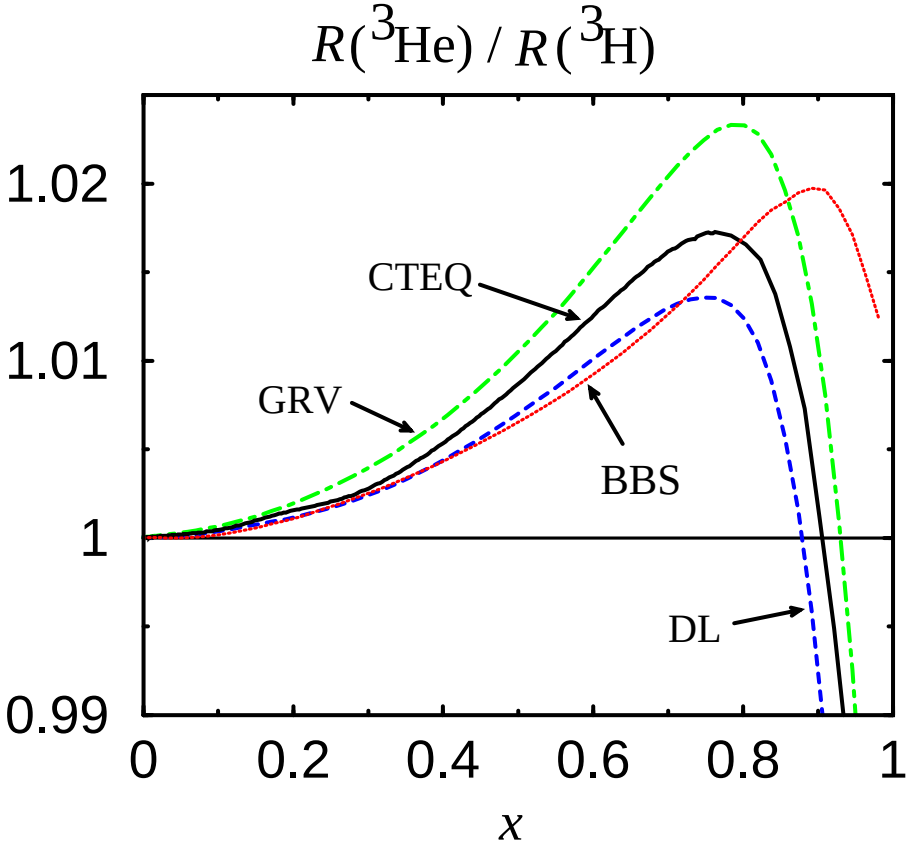

Figure 7: Ratio of nuclear EMC ratios for ^{3}He and ^{3}H with the Paris (EST) wave functions, using various nucleon structure function parametrizations [44] (see text): CTEQ (solid), GRV (dot-dashed), BBS (dotted), and DL (dashed).

Despite the seemingly strong dependence on the nucleon structure function input at very large x, this dependence is actually artificial. In practice, once the ratio $F_2^{^3\mathrm{He}}/F_2^{^3\mathrm{H}}$ is measured, one can employ an iterative procedure to eliminate this dependence altogether. Namely, after extracting F_2^n/F_2^p from the data using some calculated $\mathcal{R}$, the extracted F_2^n can then be used to compute a new $\mathcal{R}$, which is then used to extract a new and better value of F_2^n/F_2^p. This procedure is iterated until convergence is achieved and a self-consistent solution for the extracted F_2^n/F_2^p is obtained. Both Afnan *et al.* [44] and Pace *et al.* [55] have independently confirmed the convergence of this procedure.

As an illustration, we show in Figure 8 the result from Afnan *et al.* [45] for different numbers of iterations using as input $F_2^n/F_2^p = 1$. The convergence is relatively rapid — by the third iteration the extracted function is almost indistinguishable from the exact result. Although the effect on $\mathcal{R}$ from the present lack of knowledge of the nucleon structure function

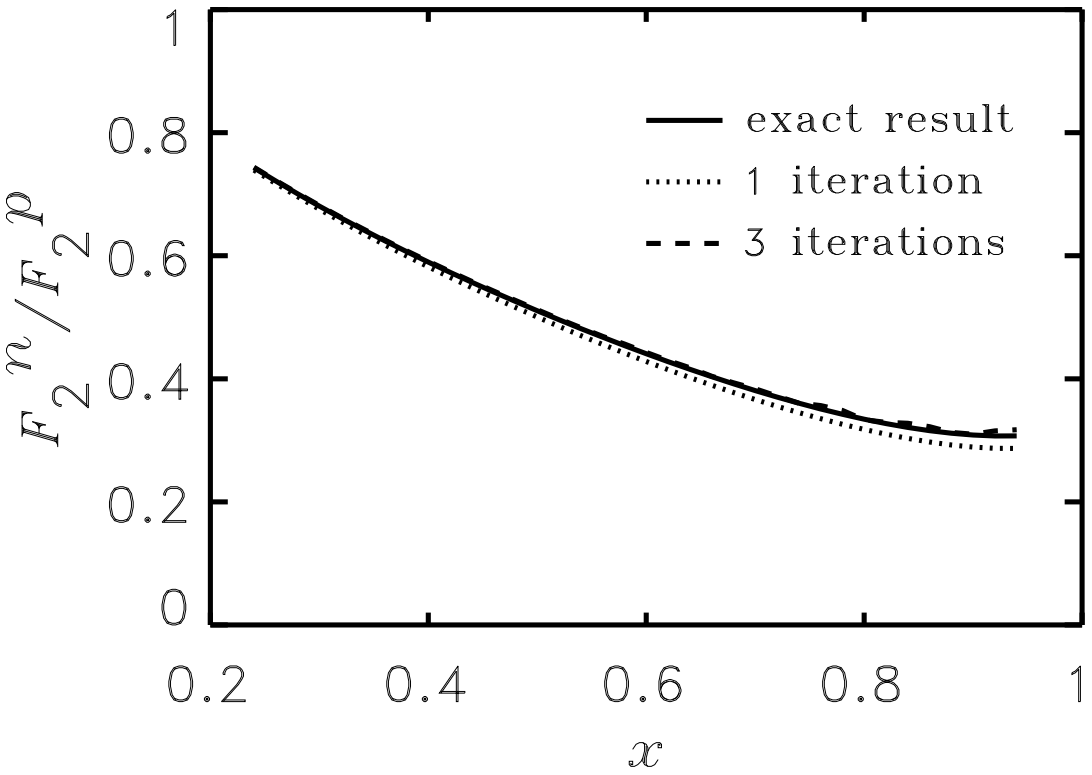

Figure 8: The convergence of the iterative procedure which eliminates the nucleon structure function dependence in the F_2^n/F_2^p extraction, from Ref. [45]. The input is $F_2^n/F_2^p = 1$, and the ratio after ~ 3 iterations is indistinguishable from the exact result (solid).

is $< 2\%$ for $x < 0.85$, this uncertainty can in principle be eliminated altogether via iteration, so that the only model dependence of $\mathcal{R}$ will be from the nuclear interaction in the $A = 3$ nucleus. An alternative iteration method was recently proposed by Kahn *et al.* [47], using an additive nuclear correction rather than the usual multiplicative *ansatz*, which has the virtue of being suitable for extracting structure functions that are not necessarily monotonic nor positive definite. Test results show that for smooth functions, very similar neutron F_2^n values are obtained with either method [47].

Of course the accuracy of the iteration procedure is only as good as the reliability of the above formalism and wave functions used to calculate the nuclear structure functions allows. The ratios in Figure 5 were calculated using three-nucleon wave functions neglecting the Coulomb interaction and working in an isospin basis (possible three-body forces can be omitted since these are expected to have a negligible effect on $\mathcal{R}$). To estimate the effect of neglecting the Coulomb interaction in ^{3}He and at the same time correct the long-range part

of the three-body wave function due to the change in the binding energy, Afnan *et al.* [45] have modified the $^1S_0$ potential in ^{3}He and ^{3}H to reproduce their respective experimental energies. In this way the $^3S_1 - ^3D_1$ interaction responsible for the formation of the deuteron is unchanged. This approximation spreads the effect of the Coulomb interaction over both the *pp* and *np* interaction in the ^{1}S$_0$ channel, and to this extent, it shifts some of the Coulomb effects in the neutron distribution in ^{3}He to the proton distribution. However, this simple modification to the $^1S_0$ interaction allows one to study explicitly the possible effects associated with the differences in the binding energies of ^{3}He and ^{3}H.

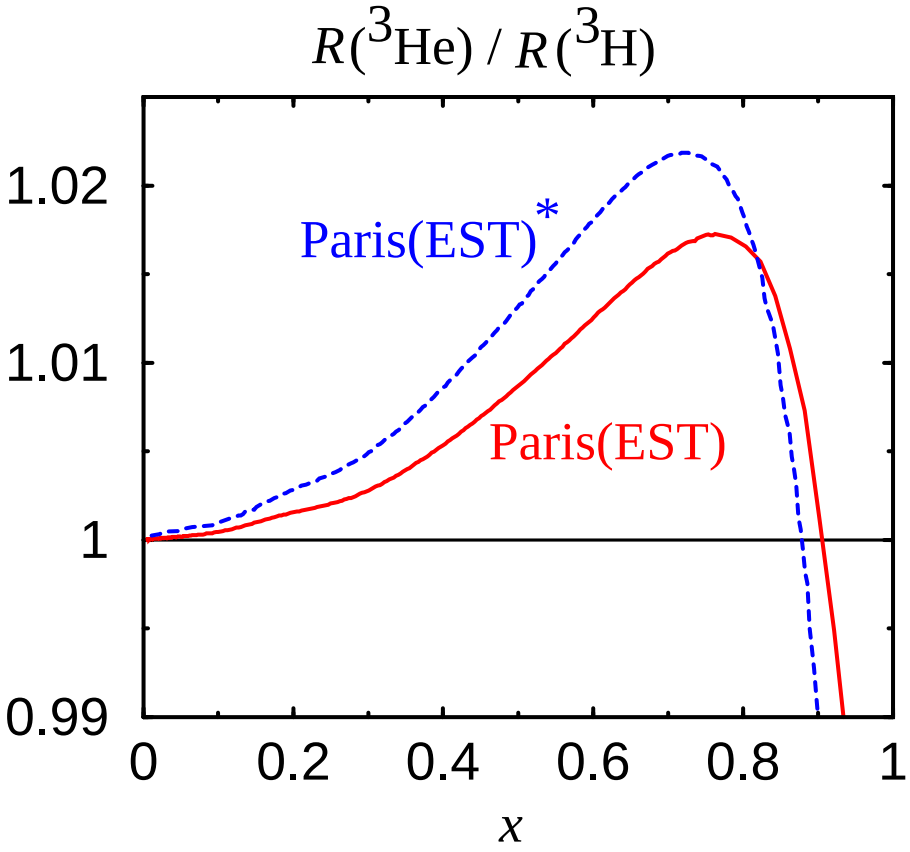

Figure 9: Ratio of nuclear EMC ratios for ^{3}He and ^{3}H for the Paris (EST) model (solid) and for the modified Paris (EST)* model (dashed) which includes explicit isospin symmetry breaking [44].

The ratio $\mathcal{R}$ calculated in Ref. [45] with the Paris (EST) wave function modified according to this prescription is shown in Figure 9, labeled "Paris (EST)*" [the CTEQ parametrization of the nucleon structure function at $Q^2 = 10$ (GeV/c)^2 is used]. The result of this modification is a shift of $< 0.5\%$ in $\mathcal{R}$, with the net effect still being a ratio which deviates by $< 2\%$ from unity.

In other models (see *e.g.* Pace *et al.* [55]) the Coulomb interaction is already included in the $A = 3$ wave functions, together with realistic two-body and three-body forces. In the actual analysis of data the uncertainty arising from the treatment of Coulomb effects will therefore be significantly smaller than that suggested by the difference between the two curves in Figure 9.

There are a number of other possible effects which could influence the ratio $\mathcal{R}$. Included in these is the Q^2 dependence of the structure functions, through higher order perturbative QCD corrections, higher twist terms, target mass corrections, and the choice of the form of the initial parton distributions. The impact of QCD corrections on the F_2^n/F_2^p ratio has been thoroughly investigated in Ref. [62]. The formalism for target mass corrections exists [63, 64] and can be readily applied to the analysis of F_2^n/F_2^p [65]. Other uncertainties are inherent to the convolution formalism in a nucleus. The derivation of the convolution approximation in Equation 17 assumes that the nucleon off-shell dependence in the bound nucleon structure function is negligible. The off-shell dependence of F_2^N is, as a matter of principle, not measurable, since one can always redefine the nuclear spectral function to absorb any p^2 dependence in the bound nucleon structure function. However, off-shell effects can be identified once a particular form of the interaction of a nucleon with the surrounding nuclear medium is specified. The discussion of off-shell modification of the nucleon structure function in the nuclear medium is therefore understood to be within the framework of the nuclear spectral functions defined in Equation 18.

Taking the nucleon's off-shellness into account, the bound nucleon structure function in Equation 17 can be generalized to [66, 67, 68]:

$$F_2^A(x,Q^2) \;=\; \int dy \int dp^2 \; \varphi(y,p^2,Q^2) \; F_2^N(x',p^2,Q^2) \; , \tag{22}$$

where $x' = x/y$ and the function $\varphi(y,p^2,Q^2)$ depends on the nuclear wave functions. In the absence of p^2 dependence in F_2^N, the light-cone momentum distribution $f(y,Q^2)$ in Equation 17 would correspond to the p^2 integral of $\varphi(y,p^2,Q^2)$. In the approach of Ref. [66], the medium-modified nucleon structure function $F_2^N(x',p^2,Q^2)$ can be evaluated in terms of a relativistic quark spectral function which depends on the virtualities of the struck quark, k^2, and spectator system. The dependence of $k_{\rm min}$ on p^2 ($\neq M^2$) generates an off-shell correction which grows with A due to the A-dependence of the virtuality p^2 of the bound nucleon. This serves to enhance the EMC effect at large x in comparison with naive binding model calculations which do not take into account nucleon off-shell effects.

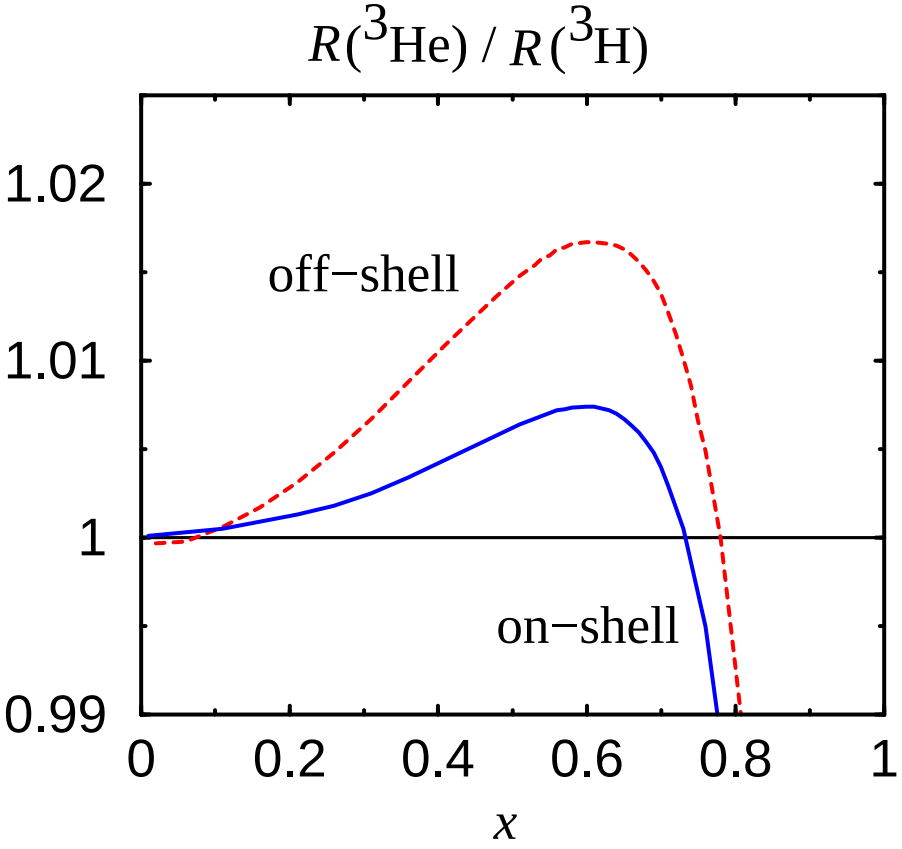

Figure 10: Ratio $\mathcal{R}$ of nuclear EMC ratios for ^{3}He and ^{3}H nuclei, with (dashed) and without (solid) nucleon off-shell corrections [66] (see text), for the variational (RSC) wave function.

The effect of the off-shell correction on the ratio $\mathcal{R}$, illustrated in Figure 10, is a small ($< 1\%$) increase in the ratio at $x \sim 0.6$. Off-shell effects of this magnitude can be expected in models of the EMC effect where the overall modification of the nuclear structure function arises from a combination of conventional nuclear physics phenomena associated with nuclear binding, and a small medium dependence of the nucleon's intrinsic structure. Other models of the EMC effect, such as the color screening model for the suppression of point-like configurations (PLC) in bound nucleons [69], attribute most or all of the EMC effect to a medium modification of the internal structure of the bound nucleon, and consequently predict larger deviations of $\mathcal{R}$ from unity [57]. However, recent ^{4}He$(\vec{e}, e'\vec{p})$ polarization transfer experiments [70] indicate that the magnitude of the off-shell deformation is indeed rather small. The measured ratio of transverse to longitudinal polarization of the ejected protons in these experiments can be related to the medium modification of the electric to magnetic elastic form factor ratio. Using model independent relations derived from quark-hadron duality, the medium modifications in the form factors were related to a modification at large x of the

deep inelastic structure function of the bound nucleon in Ref. [71]. In ^{4}He, for instance, the effect in the PLC suppression model was found [71] to be an order of magnitude larger than that allowed by the data [70], and with a different sign for $x > 0.65$. The results therefore place rather strong constraints on the size of the medium modification of the structure of the nucleon, suggesting little room for large off-shell corrections, and support a conventional nuclear physics description of the ^{3}He/^{3}H system as a reliable starting point for nuclear structure function calculations.

Corrections to the impulse approximation arising from the exchange of quarks between nucleons in $A = 3$ nuclei have been discussed by a number of authors [72, 73, 45, 57]. In Ref. [72] the effect on the EMC ratio, for the isospin-averaged $A = 3$ nucleus, was found to be comparable to that arising from binding. However, the analysis [72] did not allow for NN correlations, which are important at large momentum (and hence large x), so that the overall EMC effect is likely to have been overestimated. The effects of quarks which are not localized to single nucleons can alternatively be parametrized in terms of multi-quark clusters, in which six (or more) quarks form color singlets inside nuclei [74]. Six-quark configurations in the deuteron and other nuclei have been studied in a variety of observables, including nuclear electromagnetic form factors, NN scattering, as well as the EMC effect. Following Ref. [74], contributions from scattering off quarks in a six-quark cluster can be approximated by an effective six-quark structure function, $F_2^{6q}(x_{6q})$, in the nucleus, where $x_{6q} = Q^2/2M_{6q}\nu \approx x/2$. If P_{6q} is the probability of finding a six-quark cluster in the nucleus, the net effect on the ^{3}He (and similarly ^{3}H) structure function can be approximated by:

$$F_2^{^3\mathrm{He}} \;\longrightarrow\; (1 - P_{6q})F_2^{^3\mathrm{He}} + P_{6q}F_2^{6q} \;, \tag{23}$$

where $F_2^{^3\mathrm{He}}$ is the incoherent nucleon contribution.

For a typical valence-like shape for F_2^{6q}, with the large-x behavior constrained by hadron helicity counting rules, $F_2^{6q} \sim (1-x_{6q})^9$, Afnan *et al.* [45] have calculated the effect on $\mathcal{R}$ for $P_{6q} = 0\%$, 2% and 4%, shown in Figure 11. The overall effect is $< 1\%$ for all $x < 0.85$ even for the largest six-quark probability considered. For larger values of P_{6q} the deviation from unity is in fact even smaller, canceling some of the effects associated with nucleon off-shell dependence, for instance. Afnan *et al.* [45] and Sargsian *et al.* [57] have also considered other six-quark structure functions, and while there is some sensitivity to the exact shape of F_2^{6q}, the $\sim 1\%$ effect on $\mathcal{R}$ appears to be an approximate upper limit for all x.

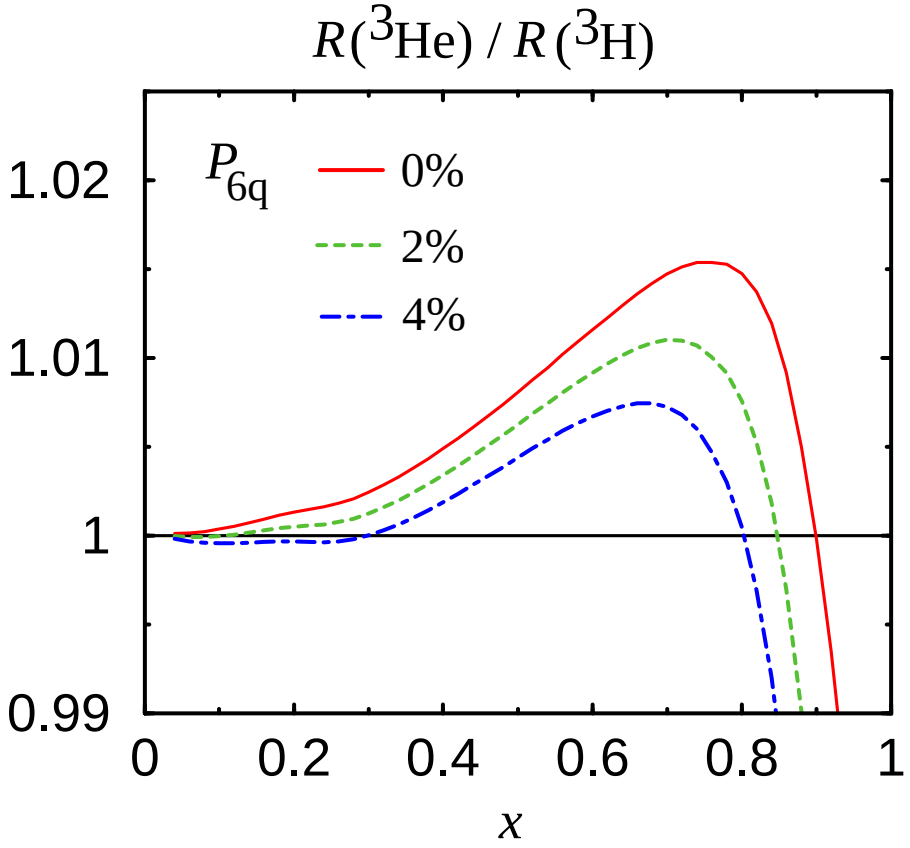

Figure 11: Ratio of nuclear EMC ratios for ^{3}He and ^{3}H for the Faddeev Paris(EST) wave function, with $P_{6q} = 0\%$, 2% and 4% six-quark configurations in the $A = 3$ wave function [45].

The analyses of the convolution model and the various extensions discussed in Refs. [44, 45, 55, 57] demonstrate the magnitude of the theoretical uncertainty in the calculation of the ratio $\mathcal{R}$. For the purpose of this proposal we assume that we can describe $\mathcal{R}$ with a central value and assign a systematic theoretical uncertainty that grows from 0.0% at $x = 0$ to $\pm 1.0\%$ at $x = 0.85$. Further theoretical investigations in the future could possibly reduce this uncertainty.

5 The Experiment

The upgraded 11 GeV beam of the Continuous Electron Beam Accelerator of Jefferson Lab offers a unique opportunity to perform deep inelastic electron scattering off the ^{3}He and ^{3}H mirror nuclei at large-x and Q^2 values. The DIS cross section for ^{3}H and ^{3}He is given in terms of their F_1 and F_2 structure functions by Equation 1. The nuclear structure functions

F_1 and F_2 are connected through the ratio $R = \sigma_L/\sigma_T$, where σ_L and σ_T are the virtual photoabsorption cross sections for longitudinally and transversely polarized photons, by:

$$F_1 = \frac{F_2(1+Q^2/\nu^2)}{2x(1+R)} \ . \tag{24}$$

The ratio R has been measured to be independent of the atomic mass number A in precise SLAC and CERN measurements using hydrogen, deuterium, iron and other nuclei [29, 75].

The direct substitution of Equation (24) into Equation (1) results in the elimination of F_1 in the inelastic cross section formula:

$$\sigma = \frac{4\alpha^2(E')^2}{Q^4}\cos^2(\frac{\theta}{2})F_2\left[\frac{1}{\nu} + \frac{(1+Q^2/\nu^2)}{xM(1+R)}\tan^2(\frac{\theta}{2})\right]. \tag{25}$$

By performing the tritium and helium measurements under identical conditions, using the same incident beam and scattered electron detection system configurations (same E, E' and θ), and assuming that the ratio R is the same for both nuclei, the ratio of the DIS cross sections for the two nuclei will provide a direct measurement of the ratio of their F_2 structure functions:

$$\frac{\sigma(^3\mathrm{H})}{\sigma(^3\mathrm{He})} = \frac{F_2(^3\mathrm{H})}{F_2(^3\mathrm{He})}. \tag{26}$$

The key technical issue for this experiment is the availability of a tritium target. Tritium targets have been used in the 1980's to measure the elastic form factors of ^{3}H at Saclay [76] and MIT-Bates [77]. The Saclay target contained liquid ^{3}H at 22 K and 20 atm (density of 0.260 g/cm^3), and had an activity of 10 kCi. The target cell was designed to have a thin wall in only one scattering direction, with the cooling head on the other side. The MIT-Bates target [78] contained gas ^{3}H at 45 K and 15 atm (density of 0.025 g/cm^3), and had an activity of 145 kCi. When not in use, the tritium gas was stored in uranium beds, a widely used commercially available technology. The target had multiple layer containment and relied on the uranium storage beds as a first defense for absorption in the event of a leak.

Given a tritium target, an entire program of elastic, quasielastic and inelastic measurements can be done at JLab [79, 80]. Also measurements of semi-inclusive DIS reactions could be possible [81]. This entire program can, overall, be better accomplished in Hall A (which is envisioned also as the Hall for special setups in the 12 GeV era) by building a "general purpose" low-activity tritium target. The availability of the Hall A BigBite Spectrometer (BBS) [82] with its very large solid angle allows us to use a low-density, low-activity (1 kCi), room-temperature, moderate-pressure target [the original 2006 proposal assumed

use of a medium-activity (5 kCi) cryogenic tritium target system (which was similar to the MIT/Bates target) in conjuction to the two Hall A High Resolution Spectrometers].

In recognition of the safety concerns related to tritium, we have chosen a design which minimizes both the amount of tritium on site and the amount of tritium handling required. There are a number of desired factors for a target to be used in this experiment: i) it should have thin walls for both left and right scattering, to allow multiple spectrometer use or coincidence scattering, ii) it should be long enough, to take advantage of a full spectrometer acceptance when used for small angle scattering or of a large-target-acceptance spectrometer like the BigBite, iii) it should be filled and sealed off site in order to minimize tritium handling on site, and iv) it should be able to withstand a high beam current.

Neither the Bates nor Saclay target would be adequately suitable for this experiment. Both were much shorter than the maximum length that can be accomodated by the BigBite and the High Resolution (at forward angles) Hall A Spectrometers. The large amount of tritium would make a Bates-style target unsuitable for JLab. The Saclay target could not be used with beam currents above 10 μA, and one scattering direction would not be accessible.

We have thus chosen to design a new target cell in the shape of a 25 cm long, 1.25 cm diameter cylinder made of Al-2219, a widely used tritium compatible alloy. This aluminum alloy has a yield strength that is larger than that of stainless steel at room temperature, and it has a much higher thermal conductivity than stainless steel. The target will be at room temperature, sealed, and at a pressure of 10 atm (density of 0.0032 g/cm^3) with a total activity of 1 kCi. All windows will be at least 0.018 in thick. The target will be filled off site, at the STAR Facility of Idaho National Lab. The amount of tritium in the cell can be determined to about 0.5% [83]. Limiting the amount of tritium to 1 kCi allows filling and shipment with standard, commonly used containers and procedures.

Two designs are currently being investigated. One design is a single-machined piece which will incorporate the five planned target cells: ^{3}He, ^{3}H, ^{2}H, ^{1}H, and empty replica. The ^{3}He, deuterium and hydrogen cells will be at 25 atm. All target densities will be known to about a 0.5% level [83]. This five-cell structure design is shown in Figure 12. A single-heat sink with water cooling will be mounted on top of the assembly. Under normal operations, with an estimated maximum beam current of 25 μA, beam heating will be about 24 W (26 W for the He target). A second design under study would use a similar construction, but with separate target cells. A detailed safety analysis and technical details of the target are given in a separate supporting document of this proposal [84].

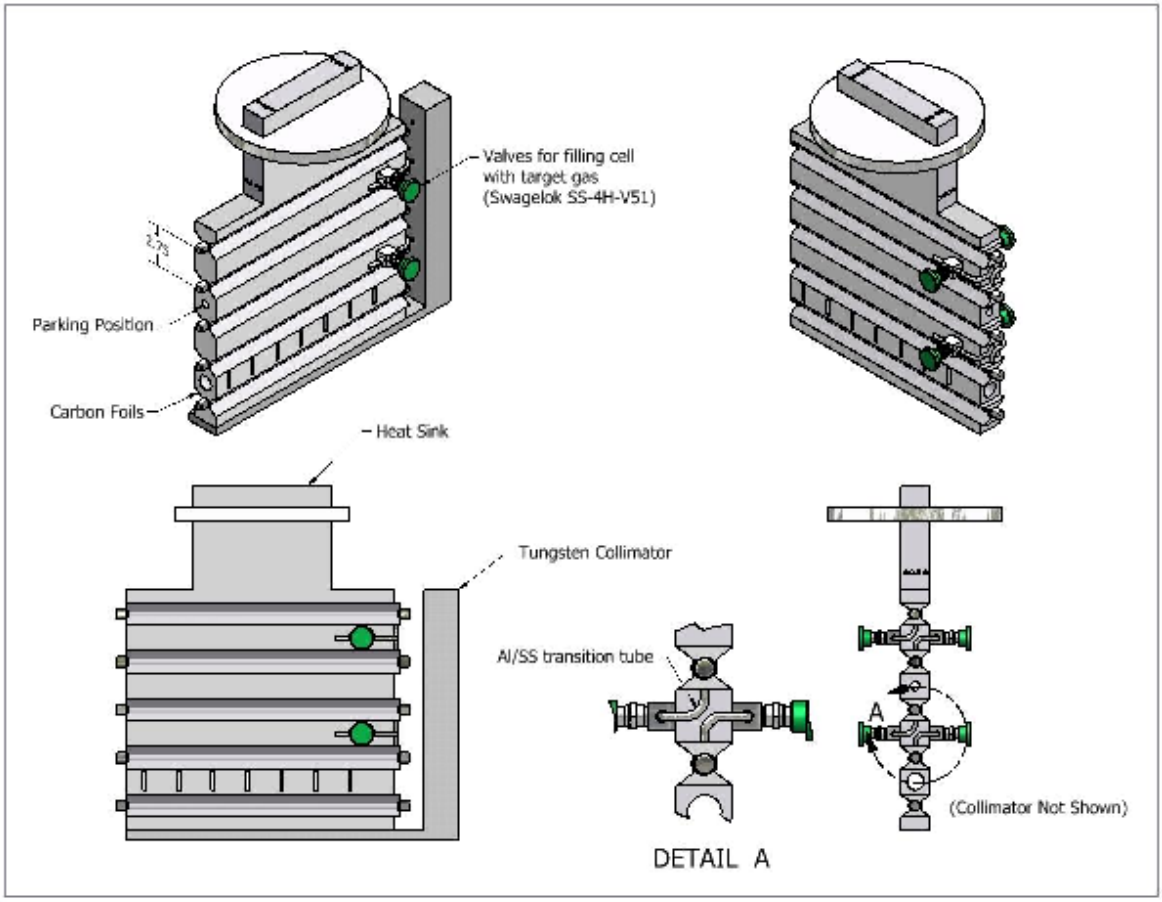

Figure 12: Schematic of the five-cell (^{3}He, ^{3}H, ^{2}H, ^{1}H, and empty replica) structure of the tritium target system (see text).

The primary safety concern for the target is a tritium leak due to mechanical failure of windows due to hydrogen embrittlement, radiation damage, or loss of target integrity from accidental excessive beam heating due to failure of the raster or grossly mis-steered beam. The alloy chosen for the target is resistant to hydrogen embrittlement at pressures below 100 atm, and the anticipated radiation exposure is at least 10^5 smaller than levels that would cause mechanical failure. In order to reduce the risk of damage from a mis-steered beam, a tungsten collimator will be placed upstream of the target. In addition to standard beam monitoring, an independent raster and steering monitor will be connected to the Fast Shut Down (FSD) system for the injector. Finite element analysis thermo-mechanical calculations have shown that the target can safely withstand either condition for at least 150 μs, enough to enable the FSD to work.

Finally, the target will be surrounded by a containment window. Any resulting leak will be vented to the outside through a system ejecting the tritium into a stack above Hall A. The resulting emission would still keep tritium levels at the site boundary below regulatory limits.

To eliminate background electrons scattering off the end-caps of the target cells, two adjustable, properly-machined tungsten collimating slits will be mounted on the support frame of the target system, right at the side of the cells. The slits will mask the spectrometer from the target end-caps, and at the same time they will define the effective target length seen by it.

The low-x cross section measurements, for which the counting rates are relatively high, can be made with the Left High Resolution Spectrometer (HRS). The standard detector package of this spectrometer will be more than adequate for the needs of the measurements. The high-x cross section measurements, for which the counting rates are relatively low, can be made with the BigBite Spectrometer, shown in Figure 13. This spectrometer will be used at large angles (greater than 42°), where backgrounds are expected to be either negligible or tolerable, based on previous Hall A experience. The BBS system is equipped with a set of drift chambers, a gas threshold Cherenkov counter, a highly-segmented scintillator plane, and a highly-segmented lead-glass electromagnetic calorimeter consisting of a preradiator and a total absorber. The BigBite has been successfully operated in previous experiments. To better understand the optical properties of BBS and to be able to develop a reliable Monte Carlo model for this experiment, we are proposing to measure the magnetic field of the dipole and produce a complete field map. Also, to minimize background to the detectors originating from the target area (which is believed to be, based on the so far BBS operational experience, the dominant source of background to the detectors [85]), we are proposing to install a collimator upstream of the dipole magnet aperture. This collimaror will be sized to prevent as many particles as possible from scattering off the BigBite poles and coils and showering into the detector stack.

All BBS detector performance has been deemed satisfactory with the exception of the Cherenkov counter, which showed a background on the phototubes of the side closer to the beam line. The low number of photoelectrons achieved (about 6-7) did not allow for a high ADC cut to reject the background without serious compromise to the detection efficiency. To overcome this problem we are proposing to increase the number of expected photoelectrons by i) increasing the radiator length from 40 cm to 70 cm and ii) recoating all the mirrors

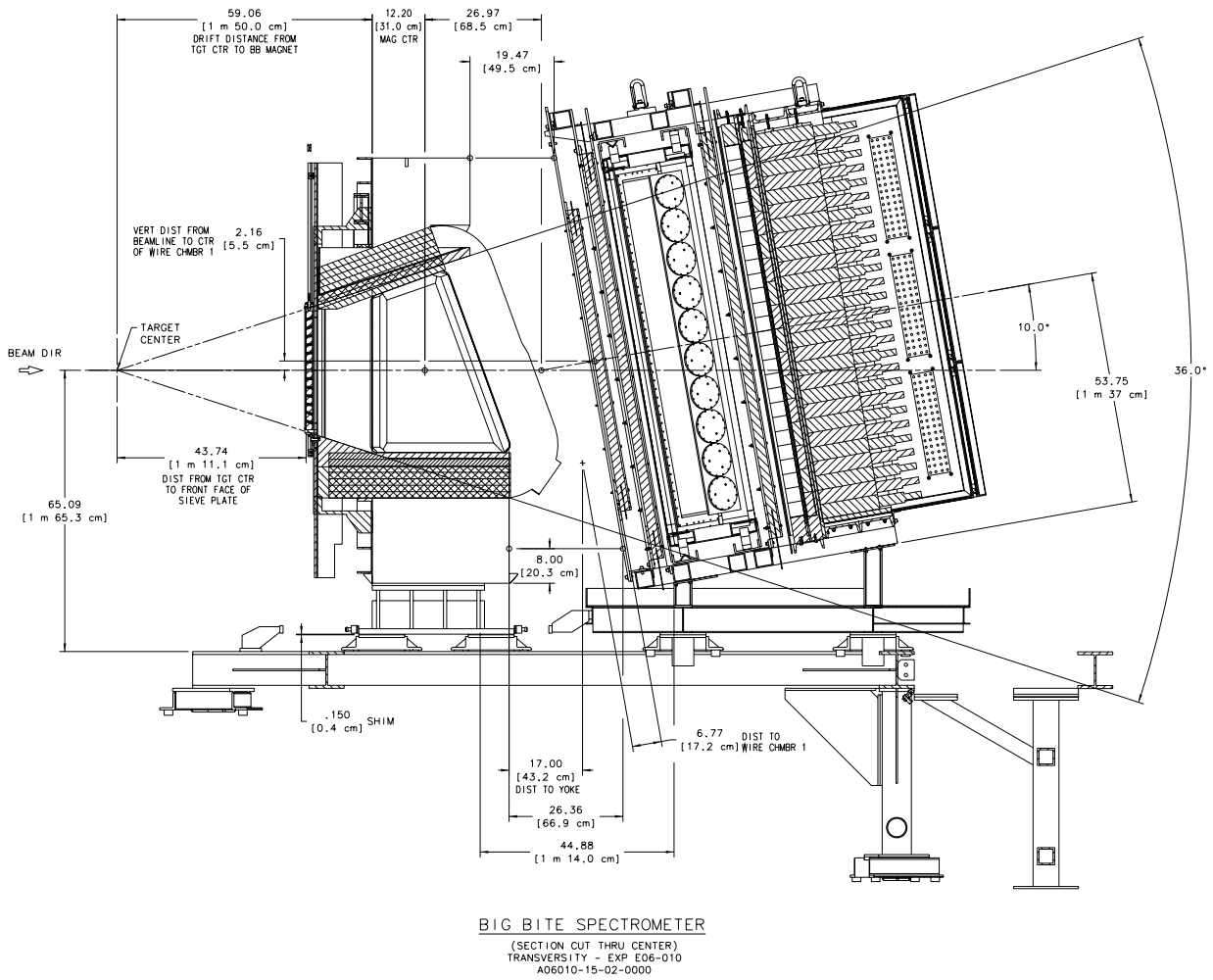

Figure 13: Side-view engineering drawing of the Hall A BigBite Spectrometer, showing its dipole magnet, the drift chambers, the Cherenkov counter, the scintillator hodoscope and the electromagnetic calorimeter (see text). In the configuration shown here, the distance between the target and the dipole face is 1.50 m. For this experiment, this distance will be reduced to 1.35 m.

as well as the Winston cones just in front of the phototubes. The recoating will be done at a specialized shop of CERN. These two modifications are expected to triple the number of photoelectrons, which will allow for a high ADC cut, if needed, which will not compromise the detection efficiency. Also, it should be mentioned that the shortening of the ADC gate from 120 ns, as previously set, to 30 ns with proper electronics timing (the width of Cherenkov signals is typically about 15 ns) can potentially significantly reduce the observed phototube background. A schematic of the BBS Cherenkov counter is given in Figure 14.

An important check would be to confirm that the ratio $R = \sigma_L/\sigma_T$ is the same for ^{3}H and ^{3}He (it is known that R is the same for hydrogen, deuterium and several medium and heavy nuclei like Be, Fe etc.). The R values will be extracted from a Rosenbluth separation of DIS cross sections, which requires a very well calibrated and understood small solid angle spectrometer like the Hall A High Resolution Spectrometer. The HRS performance is expected to be comparable, if not better, to that of the SLAC 8 GeV/c spectrometer that has provided the most precise measurements of R for hydrogen, deuterium and several medium/heavy nuclei [16, 86, 75] with overall systematic uncertainties of typically between ± 0.02 and ± 0.03. Similar R measurements at JLab in an experiment using one of the two HRS systems in Hall A will produce data of the same or smaller overall systematic uncertainties.

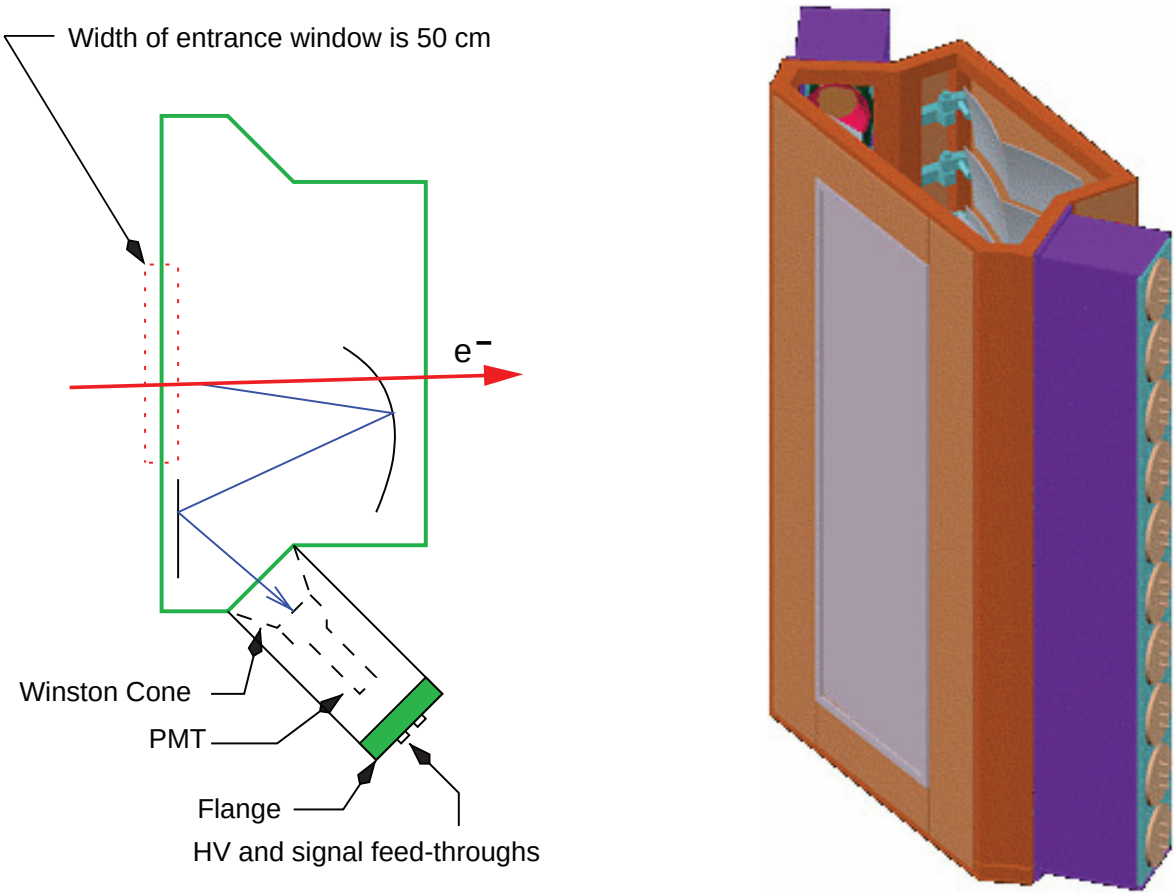

Figure 14: Cross sectional view and schematic of the Cherenkov counter of the BigBite Spectrometer. Cherenkov light is reflected from 20 spherical mirrors back to two flat mirrors and then directly or indirectly through Winston cones on the phototubes.

For the primary objective of the experiment, which is measurements of cross section ratios rather than absolute cross sections, many of the experimental errors that plague absolute

measurements will cancel out. The experimental systematic uncertainties on the ratio of cross sections should be similar to those achieved by SLAC experiments E139 [16] and E140 [86, 75], which were typically $\pm 1.0\%$ overall and $\pm 0.5\%$ point-to-point.

Inelastic scattering with electron beams up to 11 GeV at JLab can provide measurements of the ^{3}H and ^{3}He F_2 structure functions in the x range from 0.2 to 0.9. The electron scattering angle will range from 13° to 68° and the scattered electron energy from 0.6 to 4.2 GeV. As mentioned above, the cross section data will be taken with the BigBite and the Left HRS systems. Electron identification and supression of an associated hadronic (mostly pion) background will be accomplished with the Cherenkov and calorimeter packages of the two spectrometers. This standard two-counter combination has provided in the past a pion rejection factor of up to 10^5 to 1 [86] and has allowed DIS cross section measurements with negligible pion contamination up to a pion over electron ratio $\pi/e = 500$. The expected π/e ratio for this experiment has been estimated, using SLAC measurements of photon-nucleon cross sections [87], to be less than 300 for all kinematics. The pion contamination for a π/e ratio of 300 would be about 0.6%, which can be corrected with an estimated uncertainty of less than $\pm 0.2\%$. The expected π/e ratio is given in Table 1 (Appendix I) along with the kinematical parameters for the proposed core set of DIS measurements of the ratio $F_2(^3\mathrm{H})/\mathrm{F}_2(^3\mathrm{He})$ from $x = 0.23$ up to $x = 0.87$.

The estimated DIS cross sections, counting rates and the beam times required for the above core measurements are given in Table 2 (Appendix II). The deuteron DIS cross section is not given in the Table, as it is simply one third of the sum of the ^{3}He and ^{3}H cross sections (see below). The core inelastic measurements for the structure functions of ^{3}He, ^{3}H and deuterium will be away from the nucleon resonance region with $W \geq 2.0$ GeV. It will also be possible to measure the ^{3}He and ^{3}H structure functions at higher-x values over the resonance region. [The quantity W is the invariant mass of the final hadronic state: $W = (M^2 + 2M\nu - Q^2)^{1/2}$.] Earlier studies of the proton F_2^p structure function in the nucleon resonance region [88] found that Bloom-Gilman duality (equivalence of the structure function averaged over the resonance region with the deep inelastic scaling function) worked to good accuracy for Q^2 down to ~ 1 (GeV/c)^2. Phenomenological model studies [89] suggest that duality may work even better in the case of the neutron F_2^n structure function, so that for points with x greater than 0.83, the extracted F_2^n/F_2^p ratio could be interpreted in terms of the quark distribution ratio d/u. Furthermore, recent studies of ratios of nuclear cross sections at large values of x, between 0.6 and 0.8, strongly suggest that duality could be a

good approximation for the highest Q^2 achievable at JLab [90]. Therefore, we propose to take an additional kinematic point at $x = 0.87$ in the resonance region with W=1.75 GeV. The kinematical parameters, cross sections, counting rates and times for this point are also given in Tables 1 and 2.

The expected scattered electron counting rates have been estimated, under the assumption that $\sigma(^3He) \simeq \sigma_d + \sigma_p$ and $\sigma(^3H) \simeq 2\sigma_d - \sigma_p$, using values for the proton (F_2^p) and deuteron (F_2^d) structure functions and for the ratio R from the "global" analysis of the SLAC DIS data [36]. The rates assume a 55 msr BBS solid angle for a point target [which is reduced to about 45 msr and 42 msr for a 25 cm long target at 42° (smallest proposed angle) and 57° (largest proposed angle), respectively], and include, in an approximative way, losses due to radiative effects. It should be noted that the BBS solid angle is limited by the size of the detectors rather than the size of the dipole magnet aperture. It is evident from the listed rates that the proposed experiment will be able to provide very high-statistics data and perform any necessary systematic studies in a very timely fashion. The required beam times for the x-scan of the helium and tritium cross sections, listed in Table 2, are 167 and 250 hours, respectively, for a canonical beam current of 25 μA. Inelastic scattering from the deuteron will be also performed at all these kinematics, which will require 180 hours.

A very important systematic check will be to confirm, at selected kinematics, the expectation that the ratio $R = \sigma_L/\sigma_T$ is the same for ^{3}H and ^{3}He. The high beam energy of CEBAF and the momentum and angular range available by the HRS system can provide measurements of R in the same x range (0.2-0.7) as in the SLAC NPAS E140X experiment [75] by means of a Rosenbluth separation versus $\epsilon = [1+2(1+\nu^2/Q^2)\tan^2(\theta/2)]^{-1}$ (the degree of the longitudinal polarization of the virtual photon mediating the scattering). Our R measurements will be mostly limited by inherent systematics uncertainties rather than, as in the SLAC case, statistical uncertainties, and will be of the same or better precision as compared to the SLAC measurements. The large ϵ range $\Delta\epsilon > 0.50$ that can be achieved in this experiment (larger than that of SLAC) will be a decisive factor for the accuracy of these measurements. The kinematics for selected R measurements and the required beam times are given in Tables 3 (Appendix III) and 4 (Appendix IV), respectively. Five measurements of R at x = 0.25, 0.35, 0.45 and 0.55 and 0.65 with Q^2 = 1.27, 1.76, 3.04, 3.82 and 5.66 (GeV/c)^2 and W = 2.16, 2.03, 2.14, 2.00 and 1.98 GeV, respectively, will provide an excellent set of data for checking the universality of R and comparing with the world data. This set of measurements will require 3.3, 4.4, 5.5, 6.6, 7.7 and 8.8 GeV beams (with 3 of them being

straight multiples of 2.2 GeV single-pass machine configurations). The required beam time for the R measurements is 270 hours for the canonical beam current of 25 μA. Assuming an additional 10% of running with the polarity of the magnets of the spectrometers reversed ("positron running", to measure contribution to the electron scattering rate from charge symmetric processes in the target), the total beam time for the experiment will be 954 hours. An additional i) 12 hours will be required for three angle-setting changes and surveys of the

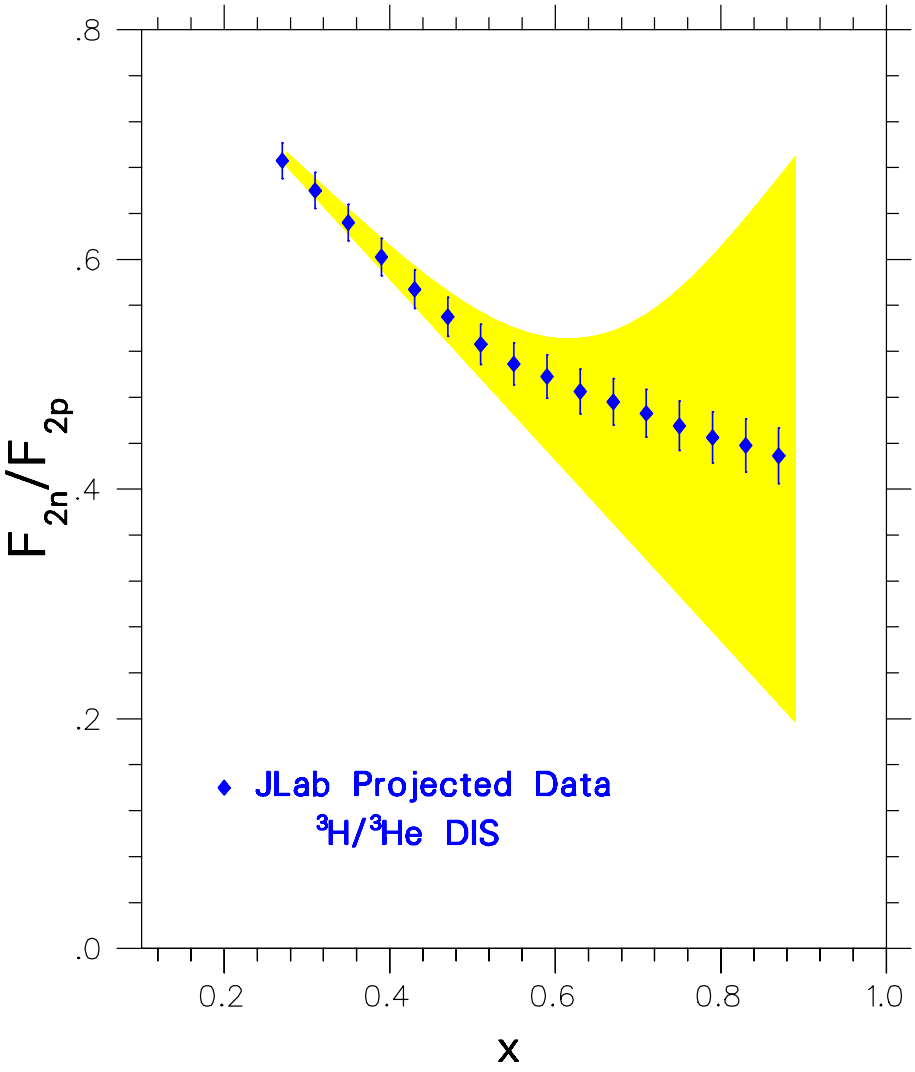

Figure 15: Projected inelastic data ($W \geq 2.0$ GeV, except for the highest-x point for which $W = 1.75$ GeV) for the F_2^n/F_2^p structure function ratio from the proposed ^{3}H/^{3}He JLab experiment with a 11 GeV electron beam. The error bars include point-to-point statistical, experimental and theoretical uncertainties, and an overall normalization uncertainty added in quadrature. The shaded band indicates the present uncertainty due mainly to possible binding effects in the deuteron.

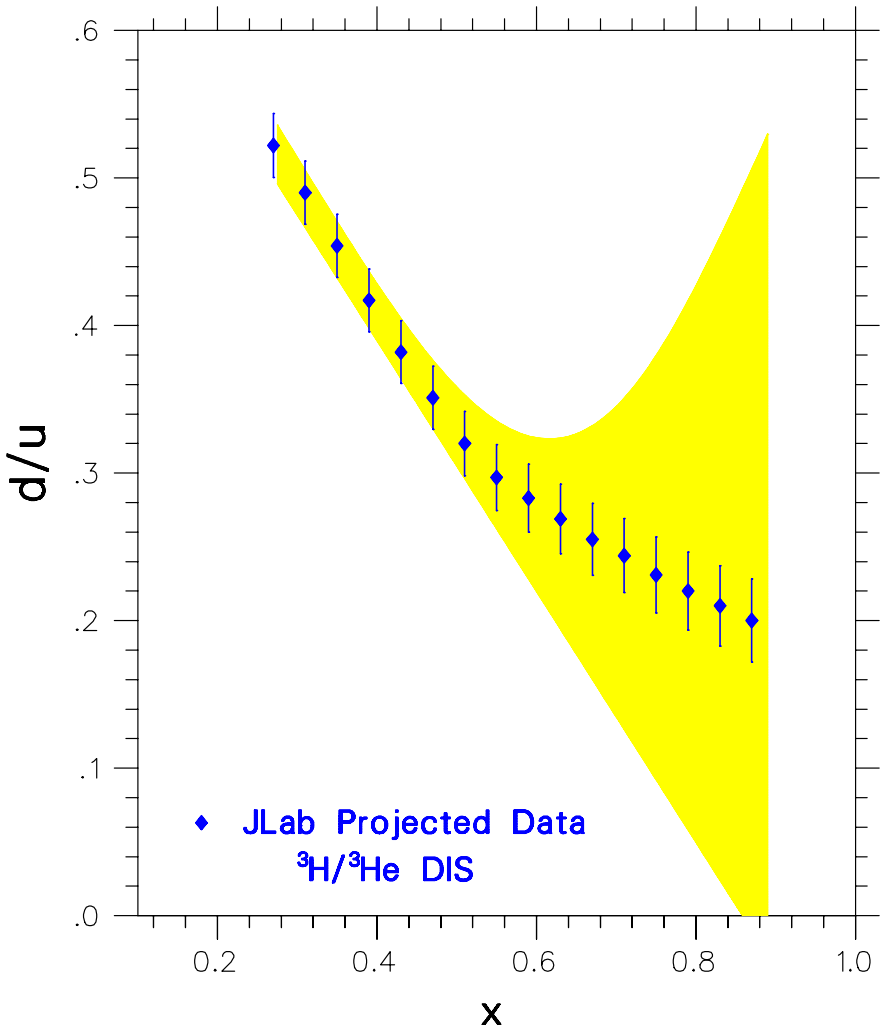

Figure 16: Projected inelastic data ($W \geq 2.0$ GeV, except for the highest-x point for which $W = 1.75$ GeV) for the d/u quark distribution ratio from the proposed ^{3}H/^{3}He JLab experiment with a 11 GeV electron beam. The error bars include point-to-point statistical, experimental and theoretical uncertainties, and an overall normalization uncertainty added in quadrature. The shaded band indicates the present uncertainty due mainly to possible binding effects in the deuteron.

BigBite Spectrometer and ii) 33 hours for changing the polarity of the HRS and BBS dipole magnets (11 manual interchanges of power cables). This bring the total experiment time to 999 hours (42 days). This total experiment time, as is customary, assumes 100% efficiency, not including detector/spectrometer checkout time, Hall A apparatus or accelerator down times etc.

6 Projected Experimental Results

The point-to-point uncertainties in the F_2^n/F_2^p determination will result from i) point-to-point uncertainties that do not cancel in the DIS cross section ratio of ^{3}H to ^{3}He ($\sim \pm 0.5\%$ as in SLAC experiment E140 [86]), ii) the theoretical uncertainty in the calculation of the super-ratio $\mathcal{R}$ (negligible at low x and growing up to $\sim \pm 1.0\%$ in the vicinity of $x = 0.85$), and iii) statistical uncertainties in the DIS cross section ratio of ^{3}H to ^{3}He (less than $\pm 1\%$). The overall normalization of the F_2^n/F_2^p ratio will be fixed by normalizing this experiment's low-x data for this ratio to the corresponding SLAC data, which at low x are free from theoretical uncertainties. The overall normalization error this way for the F_2^n/F_2^p ratio will be ± 0.01 [36].

The quality of the projected data on the F_2^n/F_2^p and d/u ratios, under the above conditions, is shown in Figures 15 and 16, respectively. The error bars include the point-to-point statistical, experimental systematic and theoretical uncertainties, and the overall normalization uncertainty, all added in quadrature. The shaded areas in Figures 15 and 16 indicate the present uncertainty, due mainly to possible nuclear corrections, in the extraction of F_2^n/F_2^p and d/u from hydrogen and deuterium inelastic data. It is evident that the proposed experiment will be able to unquestionably distinguish between the present competing extractions of the F_2^n/F_2^p and d/u ratios from proton and deuterium DIS measurements, and to determine their values with an unprecedented precision in an almost model-independent way.

It should be noted that the neutron F_2^n structure function at high x will be also measured in another Jefferson Lab 12 GeV experiment by the BoNuS Collaboration in Hall B [91] (the Collaboration has already taken data with the 6 GeV beam in JLab experiment E03-012 [92]). BoNuS relies in the detection of backward spectator protons in coincidence with the scattered electrons from the $e + d \rightarrow e + p_s + X$ inelastic reaction. The cross section for this process is factorized in terms of the deuteron spectral function S and an effective neutron F_2 structure function:

$$\frac{d\sigma}{d^3p} \sim S(y, p^2) F_2^n \left(\frac{x}{y}, p^2, Q^2 \right)_{eff}, \tag{27}$$

with:

$$y = \frac{M_d - E_s + (p_s)_z}{M_d}, \qquad p^2 = -\frac{p_t^2}{1-y} - \frac{y}{1-y} \left[M^2 - M_d^2 (1-y) \right], \tag{28}$$

where p and p_s are the struck neutron and spectator proton four-momenta (with subscripts z and t denoting longitudinal and transverse components), E_s is the proton energy and M_d is

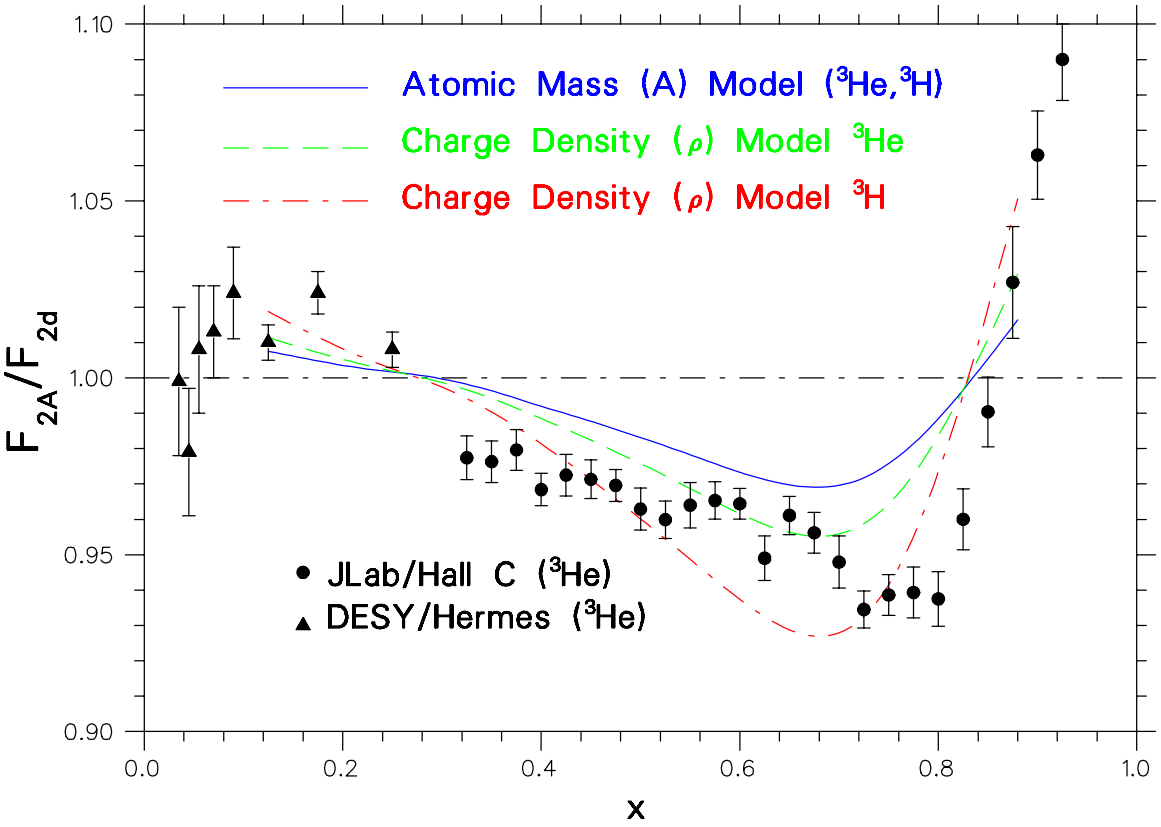

Figure 17: The ^{3}He isoscalar EMC effect ratio $F_2(^3He)/F_2(d)$ from the DESY Hermes [94] and the JLab E03-103 [95] experiments. The error bars include statistical and point-to-point systematic uncertainties added in quadrature. The $F_2(^3H)/F_2(d)$ and $F_2(^3He)/F_2(d)$ curves are based on parametrizations of SLAC data [16], assuming that the effect scales either with the atomic mass A (solid curve, ^{3}H and ^{3}He) or the nuclear charge density, ρ (dashed curve: ^{3}He, dot-dashed curve: ^{3}H). The precision of the ^{3}H/^{3}He data expected from this JLab Hall A experiment will be similar to that of the Hall C experiment on ^{3}He.

the deuteron mass. This experimental approach is based on the isolation of the modifications in the structure of the bound nucleon within the impulse approximation, by choosing kinematics to minimize effects from the deuteron wave function and final-state interactions. It relies on the selection of backward low-energy proton kinematics to minimize: i) production of low-momentum protons from quark fragmentation, and ii) final-state interactions between the spectator proton and the neutron remnant. In addition, off-shell effects appear to be minimal for $p_s < 100$ MeV/c, which is expected to minimize uncertainties arising from the extrapolation of $(F_2^n)_{eff} \rightarrow (F_2^n)_{free}$. Extensive theoretical discussions of this method are given in Refs. [69, 93].

The x-range of the BoNuS experiment for DIS scattering ($W > 2$ GeV) is not as wide as for this experiment limited to about $x = 0.77$ by the 40° maximum electron detection angle of the upgraded CLAS system. The expected statistical uncertainties on the F_2^n/F_2^p and d/u ratios are about the same for both ^{3}He/^{3}H and BoNuS experiments, and overall smaller than the systematic uncertainties. Both experiments will normalize their data on the nucleon F_2 structure function ratio to the SLAC data at low x, which are free of theoretical uncertainties. Both experiments are unequivocally highly complementary and their results are expected to be pivotal for the determination of the nucleon F_2^n/F_2^p structure function and the d/u quark distribution ratios at large values of x.

The second goal of this $A = 3$ DIS experiment is the precise determination of the EMC effect for both ^{3}H and ^{3}He at the same time, and of the ratio of the two effects. Presently, there exist only ^{3}He data, at low x from the DESY Hermes Collaboration [94], and at medium and high x (the latter over the nucleon resonance region) from the JLab Hall C Collaboration (Experiment E03-103) [95]. The existing data (which include statistical and point-to-point systematics uncertainties added in quadrature) on the isoscalar EMC effect ratio for ^{3}He are shown in Figure 17, along with two model parametrizations that describe equally well all the SLAC data for different nuclei, applied for the ^{3}He and ^{3}H cases. The solid curve in the Figure assumes that the EMC effect scales with the atomic mass number, A, and describes both $A = 3$ nuclei. The dashed and dot-dashed curves assume that the EMC effect scales with the nuclear charge density, ρ, applied to ^{3}He and ^{3}H, respectively.

This experiment will provide data on the ^{3}H EMC effect of similar precision to the Hall C E03-013 data over a similarly wide x range, as well as over wide Q^2 and W ranges for both DIS and nucleon resonance scatterings. The availability from the same experiment of also similar precision data for the ^{3}He EMC effect, will allow for an unprecedented-precision measurement of the $F_2(^3\text{H})/F_2(^3\text{He})$ ratio, where most uncertainties cancel out, providing input for the most stringest test of theoretical calculations for the EMC effect, aiming at a complete, consistent explanation of its dynamical origin.

7 Summary

We propose to perform deep inelastic electron scattering measurements off the $A = 3$ mirror nuclei using the 11 GeV upgraded beam of CEBAF and the Hall A Facility of Jefferson Lab with the BigBite Spectrometer system and one of the two HRS systems. The experiment

will require a room-temperature, moderate-pressure tritium/helium/deuterium gas target system. The required time is 42 days with beams up to mostly 11 GeV energy, and 25 μA current. The measurements will determine in an almost model-independent way the fundamental F_2^n/F_2^p structure function and d/u quark distribution ratios at high Bjorken x, and distinguish between predictions based on perturbative QCD and nonperturbative models. The precision of these measurements will provide crucial input for the improvement of parton distribution parametrizations at high x, which are needed for the interpretation of high energy hadron collider and neutrino oscillations data. The expected data will also test the validity of competing calculations of the nuclear EMC effect for the $A = 3$ systems and provide crucial constraints on theoretical models for the explanation of its dynamical origin.

References

[1] R. E. Taylor, Rev. Mod. Phys. **63**, 573 (1991).

[2] H. W. Kendall, Rev. Mod. Phys. **63**, 597 (1991).

[3] J. I. Friedman, Rev. Mod. Phys. **63**, 615 (1991).

[4] E. D. Bloom *et al.*, Phys. Rev. Lett. **23**, 930 (1969); M. Breidenbach *et al.*, Phys. Rev. Lett. **23**, 935 (1969).

[5] J. I. Friedman and H. W. Kendall, Annu. Rev. Nucl. Sci. **22**, 203 (1972).

[6] J. D. Bjorken, Phys. Rev. **179**, 1547 (1969); J. D. Bjorken and E. A. Paschos, Phys. Rev. **185**, 1975 (1969).

[7] F. E. Close, *An Introduction to Quarks and Partons*, Academic Press, London (1979).

[8] F.J. Yndurain, *Quantum Chromodynamics*, Springer-Verlag, Berlin (1983); T. Muta, *Foundations of Quantum Chromodynamics*, World Scientific, Singapore (1987).

[9] R. P. Feynman, Phys. Rev. Lett. **23**, 1415 (1969).

[10] O. Nachtmann, Nucl. Phys. **B38**, 397 (1972).

[11] A. Bodek *et al.*, Phys. Rev. Lett. **30**, 1087 (1973); E. M. Riordan *et al.*, Phys. Rev. Lett. **33**, 561 (1974); J. S. Poucher *et al.*, Phys. Rev. Lett. **32**, 118 (1974).

[12] A. Bodek *et al.*, Phys. Rev. **D20**, 1471 (1979).

[13] S. Stein *et al.*, Phys. Rev. **D12**, 1884 (1975).

[14] J. J. Aubert *et al.*, Phys. Lett. **B123**, 275 (1983).

[15] A. Bodek *et al.*, Phys. Rev. Lett. **50**, 1431 (1983); Phys. Rev. Lett. **51**, 534 (1983).

[16] J. Gomez *et al.*, Phys. Rev. **D49**, 4348 (1994).

[17] J. Kuti and V. F. Weisskopf, Phys. Rev. **D4**, 3418 (1971).

[18] F. E. Close, Phys. Lett. **B43**, 422 (1973).

[19] R. Carlitz, Phys. Lett. **B58**, 345 (1975).

[20] F. E. Close and A. W. Thomas, Phys. Lett. **B212**, 227 (1988).

[21] E. Eichten, I. Hinchliffe, K. Lane and C. Quigg, Rev. Mod. Phys. **56**, 579 (1984).

[22] M. Diemoz *et al.*, Z. Phys. **C39**, 21 (1988).

[23] A. D. Martin, R. Roberts and W. J. Stirling, Phys. Rev. **D50**, 6734 (1994).

[24] H. L. Lai *et al.*, Phys. Rev. **D51**, 4763 (1995); H. L. Lai *et al.*, Eur. Phys. J. **C12**, 375 (2000).

[25] N. Isgur, G. Karl and R. Koniuk, Phys. Rev. Lett. **41**, 1269 (1978); N. Isgur, G. Karl and D. W. L. Sprung, Phys. Rev. **D23**, 163 (1981).

[26] N. Isgur, Phys. Rev. **D59**, 034013 (1999).

[27] G. R. Farrar and D. R. Jackson, Phys. Rev. Lett. **35**, 1416 (1975).

[28] S. J. Brodsky, M. Burkardt and I. Schmidt, Nucl. Phys. **B441**, 197 (1995).

[29] D. F. Geesaman, K. Saito and A. W. Thomas, Annu. Rev. Nucl. Part. Sci. **45**, 337 (1995).

[30] P. R. Norton, Rept. Prog. Phys. **66**, 1253 (2003).

[31] A. W. Thomas, hep-ex/0007029 (2000). In Proceedings of HiX2000 Conference, Philadelphia, Pennsylvania, April 2000.

[32] G. B. West, Phys. Lett. **B37**, 509 (1971); W. B. Atwood and G. B. West, Phys. Rev. **D7**, 773 (1973).

[33] S. Liuti and F. Gross, Phys. Lett. **B356**, 157 (1995).

[34] W. Melnitchouk and A. W. Thomas, Phys. Lett. **B377**, 11 (1996).

[35] U. K. Yang and A. Bodek, Phys. Rev. Lett. **82**, 2467 (1999).

[36] L. W. Whitlow *et al.*, Phys. Lett. **B282**, 475 (1992).

[37] W. W. Buck and F. Gross, Phys. Rev. **D20**, 2361 (1979); F. Gross, J. W. Van Orden and K. Holinde, Phys. Rev. **C45**, 2094 (1992); J. Adam, F. Gross, S. Jeschonnek, P. Ulmer and J. W. Van Orden, Phys. Rev. **C66**, 044003 (2002); F. Gross and A. Stadler, Phys. Lett. B **657**, 176 (2007).

[38] W. Melnitchouk, A. W. Schreiber and A. W. Thomas, Phys. Lett. **B335**, 11 (1994).

[39] L. L. Frankfurt and M. I. Strikman, Phys. Rep. **160**, 235 (1988).

[40] M. Botje, Eur. Phys. J. **C14**, 285 (2000).

[41] S. I. Alekhin, Phys. Rev. **D63**, 094022 (2001).

[42] A. Accardi, M. E. Christy, C. E. Keppel, P. Monaghan, W. Melnitchouk, J. G. Morfin and J. F. Owens, Phys. Rev. **D81**, 034016 (2010).

[43] H. L. Lai *et al.*, Phys. Rev. **D55**, 1280 (1997).

[44] I. R. Afnan, F. Bissey, J. Gomez, A. T. Katramatou, W. Melnitchouk, G. G. Petratos and A. W. Thomas, Phys. Lett. **B493**, 36 (2000).

[45] I. R. Afnan, F. Bissey, J. Gomez, A. T. Katramatou, S. Liuti, W. Melnitchouk, G. G. Petratos and A. W. Thomas, Phys. Rev. **C68**, 035201 (2003).

[46] S. A. Kulagin and R. Petti, Nucl. Phys. A **765**, 126 (2006).

[47] Y. Kahn, W. Melnitchouk and S. A. Kulagin, Phys. Rev. **C79**, 035205 (2009).

[48] W. Melnitchouk and A. W. Thomas, Phys. Rev. **D47**, 3783 (1993) and Phys. Lett. **B317**, 437 (1993); G. Piller and W. Weise, Phys. Rep. **330**, 1 (2000).

[49] C. Ciofi degli Atti and S. Liuti, Phys. Lett. **B225**, 215 (1989); C. Ciofi degli Atti, S. Simula, L. L. Frankfurt and M. I. Strikman, Phys. Rev. **C44**, R7 (1991); S. Simula, Few Body Syst. Suppl. **9**, 466 (1995).

[50] F. Bissey, A. W. Thomas and I. R. Afnan, Phys. Rev. **C64**, 024004 (2001).

[51] C. Ciofi degli Atti, E. Pace and G. Salmè, Phys. Rev. **C21**, 805 (1980) and Phys. Lett. **B141**, 14 (1984).

[52] J. Haidenbauer and W. Plessas, Phys. Rev. **C30**, 1822 (1984).

[53] T. Y. Saito and I. R. Afnan, Few Body Syst. **18**, 101 (1995).

[54] Y. Yamaguchi, Phys. Rev. **95**, 1628 (1954).

[55] E. Pace, G. Salmè and S. Scopetta, Nucl. Phys. **A689**, 453 (2001); E. Pace, G. Salme, S. Scopetta and A. Kievsky, Phys. Rev. **C64**, 055203 (2001).

[56] S. C. Pieper and R.B. Wiringa, Ann. Rev. Nucl. Part. Sci. **51**, 53 (2001).

[57] M. M. Sargsian, S. Simula and M. I. Strikman, Phys. Rev. **C66**, 024001 (2002).

[58] C. Ciofi degli Atti and S. Liuti, Phys. Rev. **C41**, 1100 (1990) and Phys. Rev. **C44**, 1269 (1991).

[59] J. J. Aubert *et al.*, Nucl. Phys. **B293**, 740 (1987).

[60] M. Gluck, E. Reya and A. Vogt, Eur. Phys. J. **C5**, 461 (1998).

[61] A. Donnachie and P. V. Landshoff, Z. Phys. **C61**, 139 (1994).

[62] S. I. Alekhin, S. A. Kulagin and S. Liuti, Phys. Rev. **D69**, 114009 (2004).

[63] I. Schienbein *et al.*, J. Phys. **G35**, 053101 (2008).

[64] A. Accardi and J. W. Qiu, JHEP **0807**, 090 (2008).

[65] A. Accardi *et al.*, in preparation.

[66] F. Gross and S. Liuti, Phys. Rev. **C45**, 1374 (1992).

[67] W. Melnitchouk, A. W. Schreiber and A. W. Thomas, Phys. Rev. **D49**, 1183 (1994).

[68] S. A. Kulagin, W. Melnitchouk, G. Piller and W. Weise, Phys. Rev. **C52**, 932 (1995); W. Melnitchouk, G. Piller and A. W. Thomas, Phys. Lett. **B346**, 165 (1995); G. Piller, W. Melnitchouk and A. W. Thomas, Phys. Rev. **C54**, 894 (1996).

[69] L. Frankfurt and M. Strikman, Nucl. Phys. **B250**, 143 (1985);

[70] S. Dieterich *et al.*, Phys. Lett. **B500**, 47 (2001); R. Ransome, Nucl. Phys. **A699**, 360 (2002).

[71] W. Melnitchouk, K. Tsushima, A. W. Thomas, Eur. Phys. J. **A14**, 105 (2002).

[72] P. Hoodbhoy and R.L. Jaffe, Phys. Rev. **D35**, 113 (1987).

[73] M. Betz, G. Krein and T.A.J. Maris, Nucl. Phys. **A437**, 509 (1985).

[74] P.J. Mulders and A.W. Thomas, Phys. Rev. Lett. **52**, 1199 (1984); M. Sato, S. Coon, H. Pirner and J. Vary, Phys. Rev. **C33**, 1062 (1986); K.E. Lassila and U.P. Sukhatme, Phys. Lett. **B209**, 343 (1988).

[75] L. H. Tao *et al.*, Z. Phys. **C70**, 387 (1996).

[76] A. Amroun *et al.*, Nucl. Phys. **A579**, 596 (1994); F.-P. Juster *et al.* Phys. Rev. Lett. **55**, 2261 (1985).

[77] D. H. Beck *et al.*, Phys. Rev. **C30**, 1403 (1984).

[78] D. H. Beck *et al.*, Nucl. Instr. Methods in Phys. Res. **A277**, 323 (1989).

[79] J. R. Calarco, R. D. Ransome, G. G. Petratos *et al.*, in Proceedings of Workshop on Experiments with Tritium at Jefferson Lab, Newport News, Virginia, September 1999.

[80] G. G. Petratos *et al.*, nucl-ex/0010011 (2000), in Proceedings of HiX2000 Conference, Philadelphia, Pennsylvania, April 2000; R. D. Ransome, *A Tritium Program at 12 GeV*, presented at the Workshop on Physics of Nuclei with 12 GeV Electrons, Newport News, Virginia, November 2004.

[81] X. Jiang, private communication.

[82] http://hallaweb.jlab.org/equipment/BigBite/index.html; and references therein.

[83] Phil Sharpe, STAR Facility, Idaho National Lab, private communication.

[84] R. J. Holt *et al.*, *Conceptual Design of a Tritium Gas Target for Jefferson Lab*, May 2010.

[85] D. W. Higinbotham and B. Sawatsky, private communication.

[86] S. Dasu *et al.*, Phys. Rev. **D49**, 5641 (1994).

[87] D. E. Wiser, Ph.D. Thesis, University of Wisconsin (1977).

[88] I. Niculescu *et al.*, Phys. Rev. Lett. **85** (2000) 1182, 1186.

[89] F. E. Close and N. Isgur, Phys. Lett. **B509**, 81 (2001); F. E. Close and W. Melnitchouk, Phys. Rev. **C68**, 035210 (2003).

[90] J. Arrington *el.*, Phys. Rev. **C73**, 035205 (2006).

[91] S. Bueltmann *et al.* (The BoNuS Collaboration), *The Structure of the Free Neutron at Large x-Bjorken*, 12 GeV JLab Proposal E12-10-102 (2010).

[92] S. Kuhn *et al.* (The BoNuS Collaboration), *The Structure of the Free Neutron via Spectator Tagging*, JLab Proposal E03-012 (2003).

[93] S. Simula, Phys. Lett. **B387**, 245 (1996); W. Melnitchouk, M. Sargsian and M. Strikman, Z. Phys. **A359**, 99 (1997).

[94] K. Ackerstaff *et al.*, Phys. Lett. **B475**, 386 (2000); A. Airapetian, Phys. Lett. **B567**, 339 (2003).

[95] J. Seely *et al.*, Phys. Rev. Lett. **103**, 202301 (2009).

APPENDIX I

DIS Kinematics for the F_2^n/F_2^p and d/u Extraction

x	W (GeV)	Q^2 [(GeV/c)^2]	E (GeV)	E' (GeV)	θ (deg)	π/e	Spectrometer
0.87	1.75	14.6	11.0	2.07	47.1	11	BBS
0.83	1.98	14.8	11.0	1.48	57.1	92	BBS
0.79	2.16	14.2	11.0	1.41	57.1	121	BBS
0.75	2.30	13.3	11.0	1.58	51.9	66	BBS
0.71	2.45	12.7	11.0	1.50	51.9	89	BBS
0.67	2.58	11.7	11.0	1.67	47.1	52	BBS
0.63	2.68	10.8	11.0	1.90	42.0	27	BBS
0.59	2.82	10.2	11.0	1.80	42.0	39	BBS
0.55	2.60	7.22	11.0	4.00	23.4	1	HRS
0.51	2.71	6.70	11.0	4.00	22.5	1	HRS
0.47	2.80	6.17	11.0	4.00	21.6	1	HRS
0.43	2.89	5.65	11.0	4.00	20.6	1	HRS
0.39	2.98	5.12	11.0	4.00	19.6	1	HRS
0.35	3.07	4.60	11.0	4.00	18.6	2	HRS
0.31	3.15	4.07	11.0	4.00	17.5	2	HRS
0.27	3.24	3.55	11.0	4.00	16.3	3	HRS
0.23	3.32	3.02	11.0	4.00	15.1	3	HRS

Table 1: The kinematics for the proposed ^{3}He, ^{3}H and deuterium inelastic cross section measurements for the extraction of the F_2^n/F_2^p and d/u ratios as a function of the Bjorken x. The beam energy, E, is fixed at 11.0 GeV. Here, W is the invariant mass of the final hadronic state, Q^2 is minus the four-momentum transfer squared, E' is the scattered electron energy, θ is the scattered electron angle and π/e is the expected pion to electron counting ratio. Also shown is the spectrometer system (BigBite or High Resolution) which will be used at each kinematics.

APPENDIX II

Cross Sections and Counting Rates for the F_2^n/F_2^p and d/u Extraction

x	$\sigma(^3\mathrm{He})$ $(\frac{\mathrm{nb}}{\mathrm{sr}\cdot\mathrm{GeV}})$	$\sigma(^3\mathrm{H})$ $(\frac{\mathrm{nb}}{\mathrm{sr}\cdot\mathrm{GeV}})$	$CR(^3\mathrm{He})$ (e/h)	$CR(^3\mathrm{H})$ (e/h)	$CR(\mathrm{D})$ (e/h)	$t(^3\mathrm{He})$ (h)	$t(^3\mathrm{H})$ (h)	$t(\mathrm{D})$ (h)
0.87	0.0058	0.0050	459	311	433	55	79	58
0.83	0.0067	0.0055	409	263	376	66	103	72
0.79	0.0117	0.0093	713	439	644	concurrent	with	x=0.83
0.75	0.0242	0.0188	1681	1020	1504	24	38	27
0.71	0.0370	0.0285	2561	1541	2285	concurrent	with	x=0.75
0.67	0.0698	0.0537	5521	3317	4929	concurrent	with	x=0.87
0.63	0.134	0.103	12230	7347	10940	7	11	8
0.59	0.183	0.143	16670	10180	15040	concurrent	with	x=0.63
0.55	1.60	1.27	33180	20580	30060	4	5	4
0.51	2.31	1.85	49370	30890	44990	3	4	3
0.47	3.28	2.67	72300	45980	66100	2	3	2
0.43	4.64	3.83	105500	68040	97110	1	2	1
0.39	6.52	5.48	153000	100500	142200	1	1	1
0.35	9.18	7.85	222600	148700	208600	1	1	1
0.31	13.0	11.3	325400	221000	307500	1	1	1
0.27	18.7	16.6	482900	334900	457500	1	1	1
0.23	27.5	24.8	732200	515900	701600	1	1	1

Table 2: Electron DIS cross sections, counting rates (CR) and beam times (t) for the different Bjorken x kinematics of the proposed ^{3}He, ^{3}H and deuterium (D) inelastic cross section measurements for the extraction of the F_2^n/F_2^p and d/u ratios using the BBS (x=0.59-0.87) and Left HRS (x=0.23-0.55) systems. The counting rates assume 25 cm, room temperature ^{3}He (25 atm), ^{3}H (10 atm) and deuterium (25 atm) gas targets and a beam current of 25 μA.

APPENDIX III

DIS Kinematics for the $\mathbf{R = \sigma_L/\sigma_T}$ Measurements

x	ϵ	W (GeV)	Q^2 [(GeV/c)^2]	E (GeV)	E' (GeV)	θ (deg)	π/e
0.25	0.86	2.16	1.27	6.6	3.90	12.7	1
0.25	0.78	2.16	1.27	5.5	2.80	16.5	1
0.25	0.63	2.16	1.27	4.4	1.70	23.7	7
0.25	0.28	2.16	1.27	3.3	0.60	47.1	157
0.35	0.85	2.03	1.76	6.6	3.92	15.0	1
0.35	0.77	2.03	1.76	5.5	2.82	19.4	1
0.35	0.62	2.03	1.76	4.4	1.72	27.8	5
0.35	0.27	2.03	1.76	3.3	0.62	55.0	147
0.45	0.79	2.14	3.04	7.7	4.00	17.9	1
0.45	0.70	2.14	3.04	6.6	3.00	22.6	1
0.45	0.55	2.14	3.04	5.5	1.90	31.3	6
0.45	0.26	2.14	3.04	4.4	0.80	55.4	140
0.55	0.77	2.00	3.82	7.7	4.00	20.3	1
0.55	0.68	2.00	3.82	6.6	2.90	25.8	1
0.55	0.50	2.00	3.82	5.5	1.80	36.2	6
0.55	0.19	2.00	3.82	4.4	0.70	67.7	267
0.65	0.72	1.98	5.66	8.8	4.16	22.7	1
0.65	0.62	1.98	5.66	7.7	3.05	28.4	1
0.65	0.46	1.98	5.66	6.6	1.95	38.8	5
0.65	0.19	1.98	5.66	5.5	0.85	66.8	234

Table 3: The kinematics for the proposed measurements of the $R = \sigma_L/\sigma_T$ ratio for ^{3}He and ^{3}H. Here, x is the Bjorken scaling variable, ϵ is the degree of the longitudinal polarization of the virtual photon, W is the invariant mass of the final hadronic state, Q^2 is minus the four-momentum transfer squared, E and E' are the incident and scattered electron energies, θ is the scattered electron angle and π/e is the expected pion to electron counting ratio.

APPENDIX IV

Rates and Times for the $\mathbf{R = \sigma_L/\sigma_T}$ Measurements

x	ϵ	^{3}He Rate (e/h)	^{3}H Rate (e/h)	^{3}He Time (h)	^{3}H Time (h)
0.25	0.86	5826000	4104000	1	1
0.25	0.78	2594000	1833000	1	1
0.25	0.63	813500	574700	1	1
0.25	0.28	65320	46330	1	1
0.35	0.85	2475000	1690000	1	1
0.35	0.77	1099000	747900	1	1
0.35	0.62	344400	234300	1	1
0.35	0.27	25080	17080	2	3
0.45	0.79	520000	337700	1	1
0.45	0.70	244700	158700	1	1
0.45	0.55	86610	56280	1	1
0.45	0.26	8767	5703	5	7
0.55	0.77	188000	11790	1	1
0.55	0.68	86470	54430	1	1
0.55	0.50	25680	16230	2	3
0.55	0.19	2259	1423	18	28
0.65	0.72	40990	24950	1	2
0.65	0.62	19170	11950	2	4
0.65	0.46	5995	3640	7	11
0.65	0.19	720	437	57	94

Table 4: Counting rates and beam times for the ^{3}He and ^{3}H measurements of the $R = \sigma_L/\sigma_T$ ratio. Here, x is the Bjorken scaling variable and ϵ is the degree of the longitudinal polarization of the virtual photon. The counting rates assume use of the Left HRS system with moderate-pressure, room-temperature gas ^{3}He (25 atm) and ^{3}H (10 atm) targets, and a beam current of 25 μA.